Artificial simulation of the aqueous humor dynamics of the conventional outflow pathway under physiological and pathological conditions

Edward Rickie Lim Chu

Doheny Eye Institute, Los Angeles, USA

The Australian School of Advanced Medicine,

Macquarie University, Australia

November 2015

A thesis submitted in fulfillment of the requirements

for the degree of Master of Philosophy

Table of Contents

Abstract

Glaucoma is the leading cause of irreversible blindness in the world and remains a devastating ophthalmic condition. Current management seems limited and focuses mainly on reducing intraocular pressure. Glaucoma research models such as cell and organ based culture, computer simulation and animal models have played major roles in advancing the field, however, disease progression still occurs indicative that the pathophysiology of glaucoma has not been fully elucidated. In an attempt to shed some light into this issue, a novel artificial hydraulic model has been developed to empirically simulate fluid dynamics of the human conventional outflow pathway. Using non-biological materials, this model comprised of critical elements of the human aqueous outflow tract that include a microsyringe pump (simulating aqueous inflow/outflow), 35-gauge needle (stimulating trabecular meshwork), one-way valve (simulating Schlemm's canal inner wall endothelia) and a distal fluid column (simulating episcleral venous pressure) interconnected in between by pressure transducers and rigid tubings. The model was able to replicate various components of the conventional outflow pathway under physiological and pathological conditions. This system can potentially provide options to incorporate biological materials (i.e. cell cultures), include a parallel uveoscleral outflow system and/or simulate collector channel resistance to create a more comprehensive model to further our understanding in aqueous outflow dynamics.

Statement of Candidate

I certify that the work in this thesis entitled “Artificial simulation of the aqueous humor dynamics of the conventional outflow pathway under physiological and pathological conditions” has not previously been submitted for a degree nor has it been submitted as part of requirements for a degree to any other university or institution other than Macquarie University.

I also certify that the thesis is an original piece of research and it has been written by me. Any help and assistance that I have received in my research work and the preparation of the thesis itself have been appropriately acknowledged.

In addition, I certify that all information sources and literature used are indicated in the thesis.

Edward Rickie Lim Chu ID: 43467903 Date: November 14, 2015

Abbreviations

µl	microliter
η	viscosity
C_{trab}	outflow facility through trabecular route
CV	coefficient of variation
DPBS	Dulbecco's Phosphate Buffered Saline
ECM	extracellular matrix
EVP	episcleral venous pressure
F	aqueous inflow into the trabecular pathway
G	gauge
IOP	intraocular pressure
I/O	input/output
JC	juxtacanalicular
L	length
MIGS	microinvasive glaucoma surgery
P_e	episcleral venous pressure
P_i	intraocular pressure
PT	pressure transducer
R	resistance
r	radius
SC	Schlemm's canal
SEM	standard error of mean
IW	inner wall
TM	trabecular meshwork
V	volts

Acknowledgements

I express my deepest gratitude to my supervisor at the Doheny Eye Institute, Dr. James Tan for his endless guidance, patience, encouragement and wealth of knowledge. Not only is he my mentor but also one of the inspirational figures in my career. He also provided me the opportunity to work in his laboratory and introduced aqueous humor dynamics research.

I thank my supervisor at Macquarie University, Professor Stuart Graham for his support, trust and advice throughout this Masters degree.

I am very grateful to my other mentors and inspirational figures in my career, Professor Alfredo Sadun and Fred Ross-Cisneros from the Sadun Neuro-Ophthalmology Laboratory of the Doheny Eye Institute, for their advice, encouragement and support in pursuing aqueous humor dynamics research.

I also thank my laboratory colleagues, Dr. Jose Gonzalez, Dr. MinHee Ko and Dr. Michelle Kim for their assistance during experiments, brilliant ideas during brainstorming and providing support especially during times when I was venting out frustrations.

Most importantly, I am so grateful to my wife, Sigrid and son, Sebastian for their unconditional love and utmost understanding to support my journey towards this Masters degree.

Again, I thank everyone. Without any one of you, this thesis would not be possible.

Chapter 1: Introduction

Glaucoma is the second most common cause of blindness in the world after cataracts.[1,2] By 2020, it has been estimated that almost 80 million people worldwide will be affected with glaucoma and at least 11 million people (approximately 14%) will be blind in both eyes.[1] This makes glaucoma the leading cause of irreversible blindness when compared to other ophthalmic conditions.[3,4] Glaucoma is an optic neuropathy characterized by gradual loss of retinal ganglion cells in the inner retina and axons in the optic nerve that can be present in one or both eyes.[3,5] The damage is evidently associated with optic disc changes, visual field loss and sometimes, increase in intraocular pressure (IOP).[5] Typically speaking, there are a number of risk factors for glaucoma such as increasing age, ethnicity, family history of glaucoma and myopia but the only modifiable risk factor so far is elevated IOP.[3,6] In terms of glaucoma, this thesis investigates two broad categories: glaucoma with increased trabecular meshwork (TM) resistance and secondary glaucoma due to elevated episcleral venous pressure (EVP).

Intraocular pressure is determined by the equilibrium between aqueous humor production from the ciliary body and outflow via two pathways, conventional and uveoscleral. Eighty percent of total aqueous humor passes through the conventional or main outflow pathway[7], which is the main focus of this thesis. Structures of this pathway (arranged in series) include the following: TM, Schlemm's canal (SC) inner wall (IW) endothelia, SC, collector channels and exits the eye via the episcleral venous system. The remaining aqueous humor (20%) flows through the uveoscleral tract, specifically through the iris root and ciliary muscle into several other areas including across the sclera, within the supraciliary and suprachoroidal spaces,

through emissarial canals, into choroidal vessels, vortex veins and returns into the ciliary processes.[7,8] Recently, by measuring the uveoscleral outflow rate with fluorophotometry, several studies have demonstrated that the contribution of the uveoscleral tract to the total aqueous flow was higher (between 32-46% in older population (with mean age of 55 years old and older) and up to 56% in younger individuals (between 20-30 years old))[9-11] than what was previously reported.[7] The level of IOP is contributed by the resistance generated by the TM specifically within the distal juxtacanalicular (JC) region and the adjacent endothelia of the IW of the SC.[12-19] In non-glaucomatous eyes, outflow occurs when a pressure head generated by the differential between IOP and EVP is sufficient to overcome tissue resistance.[20] Occurrence of outflow could be predicted by the classic Goldmann's equation,[21,22] which models passive bulk flow of aqueous humor through the TM down a pressure gradient. The simple hydraulic model for conventional or trabecular outflow is expressed as:

$$F=C_{trab}(P_i-P_e)$$

wherein F: aqueous inflow into the trabecular pathway; C_{trab}: outflow facility through trabecular route; P_i: IOP; and P_e: EVP. This equation does not account for the uveoscleral outflow and should not be confused with the modifed Goldmann's equation. At steady state, total aqueous inflow into the trabecular pathway equals outflow by the same pathway. In glaucoma, abnormal build up of resistance in the TM/SC IW area to fluid outflow resulted to pathologically elevated IOP.[18,23]

Current treatment philosophy for glaucoma is mainly targeted on reducing IOP, which has shown to decrease the risk and progression of glaucoma.[24,25] Topical medications are generally considered first-line treatment.[3] If medical therapy was

inadequate, other options may include laser (i.e. laser trabeculoplasty), microinvasive glaucoma surgery (MIGS), incisional surgery (i.e. trabeculectomy) or aqueous shunt surgery.[3] Currently, pilocarpine, a muscarinic (cholinergic) receptor agonist, is the only topical therapy that targets the conventional outflow pathway.[8,26] This medication stimulates the parasympathetic nervous system causing ciliary muscle contraction and posterior displacement of the scleral spur, resulting in trabecular lamella enlargement and widening of the SC, eventually increasing outflow facility.[8,26] The use of pilocarpine has been limited for the following reasons: (1) poor compliance due to frequency of dosing (up to 6 times a day) and (2) side effects such as accommodative spasm, miosis, reduced visual acuity in poor lit environments and periorbital headaches.[8,26] There is also a new class of medication that targets this pathway, specifically by regulating contractile tone of the smooth muscle tissue of the TM, called Rho-associated kinase inhibitor.[27] However, this medication has only been approved in Japan and is still undergoing clinical trials in the United States.[27,28]

Numerous research methodologies have been used to advance the field of glaucoma. Concurrent ideas of deconstructing the aqueous drainage system to isolate and separately study components of interest in the outflow tract have led to the following reductionistic models: (1) cell culture; (2) *ex vivo* anterior segment organ culture system; (3) flow-through chambers with cultured TM cells; (4) computer simulation and; (5) animal models.

Monolayer TM cells cultured on artificial substrates are valuable in studying individual cellular properties[29-33] such as response to medications (i.e. prolonged glucocorticoid exposure inducing myocilin, a protein involved in primary open angle

glaucoma),[34] response to proteins (i.e. transforming growth factor beta 1 increases myocilin/trabecular meshwork inducible glucocorticoid response protein)[35] or observation of changes in physical characteristics (i.e. alteration of actin cytoskeletal network of the TM from mechanical stretching).[36,37] However, the human TM is a 3-dimensional structure made up of cells and extracellular matrix (ECM) arranged in a laminar pattern. Since cell cultures are done on a flat surface, difference in spatial arrangement *in vitro* can alter biochemical signals and cellular replication, eventually differing from cells' *in vivo* characteristics.[38,39]

Ex vivo anterior segment organ culture system are used to study the trabecular drainage system in the absence of uveoscleral outflow.[38,40-42] This approach provided a robust specimen for perfusion studies and in general, also allowed preservation of cells in its innate environment with its neighboring cells and surrounding ECM mimicking a more *in vivo* milieu compared to cell cultures.[39] Nevertheless, similar to cell cultures, *in vitro* cellular behavior and dedifferentiation as well as tissue reorganization may differ from an *in vivo* environment.[38,39] Furthermore, this technique can result to tissue distortion from manipulation.[38]

Flow-through chambers with cultured TM cells to study a different cellular environment has shown limited success with commercially available filters.[43] Recently, Torrejon *et al* developed a model that involved multiple layers of human TM cells grown on a bioengineered scaffold to mimic *in vivo* environment.[44] Furthermore, the scaffold was incorporated into a perfusion system, underwent constant flow perfusion and elicited pressure at different flow rates.

Computer simulation was used to model the drainage system's fluid mechanics.[45,46] Ethier *et al* suggested that extracellular glycosaminoglycans or proteoglycan gel in the JC meshwork is a major determinant of outflow resistance.[45] Recently, a 3-dimensional model was developed to simulate healthy and glaucomatous eyes in humans including the effects of filtering surgery.[46] However, it has shortcomings as images taken to create the simulation was based on light microscopy, which has low resolution and can lead to exclusion of fine details.

Animal models have been used to study aqueous outflow dynamics and test potential medication for glaucoma such as latrunculin, which targets TM's actin cytoskeleton.[47-49] Classically, these experiments were done on non-human primates [50-52] but more recently, live mice are used, given similarities with human eyes such as outflow pathway morphology and physiological characteristics (i.e. lowering IOP with medication).[53-55] Apart from being readily available and inexpensive, certain genetic strains of mice associated with aspects that contribute to the development of glaucoma (i.e. elevated IOP) are also available.[56-58] Limitations however, include uncooperative animals, high cost and limited availability (specifically for non-human primates), need for sedation that can affect IOP measurements[59-63] and occurrence of washout effect. This effect occurs when outflow facility increased with continuous perfusion, which was observed in live primates[64,65] but not in live mice[49] and human eyes.[66,67]

Even with these pre-existing treatments and advancement of glaucoma research models, patients still experienced disease progression and eventually irreversible blindness. This indicates that better understanding of the pathophysiology

of glaucoma affecting outflow pathway is crucial in developing new therapies. As mentioned earlier, the TM/SC IW endothelia contribute the majority of resistance in the conventional outflow pathway but the specific site remains elusive.[12-19,45] One might wonder if elucidating this question would help determine the exact nature of glaucoma. In an attempt to shed some light into this question, a novel artificial hydraulic model using non-biological materials was developed to empirically simulate fluid dynamics in both physiological and pathological scenarios of the human conventional aqueous outflow system. The model comprises of critical elements of the human aqueous drainage tract, which are combined in a way that permits each element of the perfusion system to be replicated, varied, measured and directly observed with respect to fluid dynamics. Apart from simulating the TM and SC IW endothelia separately, this model is unique as it allows measurement of simulated tissue pressure between the TM and SC IW interface. To our knowledge, this aspect of the model has never been done previously. This model is also versatile as it allows certain parts to be modified by increasing TM resistance and EVP, to recreate pathological conditions of the conventional outflow pathway. Furthermore, this model is scalable as it provides options for including features such as cellular systems (e.g. TM and SC IW cells), addition of a parallel uveoscleral outflow system or to extend the perfusion system to simulate the collector channel resistance, to more comprehensively model outflow dynamics. Herein, describes this core conventional outflow model, baseline characteristics, changes following modification of various components to simulate glaucomatous eyes and its validation with reference to the classic Goldmann's equation. The aim of this research is to strengthen our understanding of the interaction of the different parts, variation of disease parameters

and pathophysiology of this pathway, which in some ways is not possible in live animals or humans.

Chapter 2: Materials and methods

2.1 Simulation of conventional aqueous outflow dynamics under physiological conditions from an artificial hydraulic model

2.1.1 System components

The hydraulic model (Figure 1) incorporated the following components to simulate fluid dynamics within the conventional outflow pathway: (1) calibrated 50µl glass microsyringe (Hamilton 1705TLL; Hamilton Inc., Reno, NV) driven by a microsyringe pump (PhD Ultra; Harvard Apparatus, Holliston, MA) representing aqueous inflow (equalling aqueous outflow when IOP>EVP; see later); (2) a chamber representing the anterior chamber connected to a pressure transducer (PT#1). (3) PT#1 measured pressure simulating IOP in the chamber; (4) 35 gauge (G) needle (5 mm long with 127µm internal diameter; Medicom, Lachine, Quebec, Canada) simulating the TM resistor; (5) a second chamber in the series and beyond the resistor representing the TM tissue compartment was connected to (6) a second pressure transducer (PT#2) that measured tissue compartment pressure; (7) a one-way pressure control valve (Qosina Check Valve 80067, Edgewood, NY; opening pressure 7.4mmHg) representing the SC IW endothelium barrier; (8) a third chamber beyond the SC IW representing the SC chamber; (9) this chamber was connected to a third pressure transducer (PT#3) that measured EVP immediately beyond SC IW; and (10) a distal variable height fluid column providing hydrostatic pressure in SC independently of pressure generated by the microsyringe pump. The hydrostatic pressure generated by the column represented EVP.

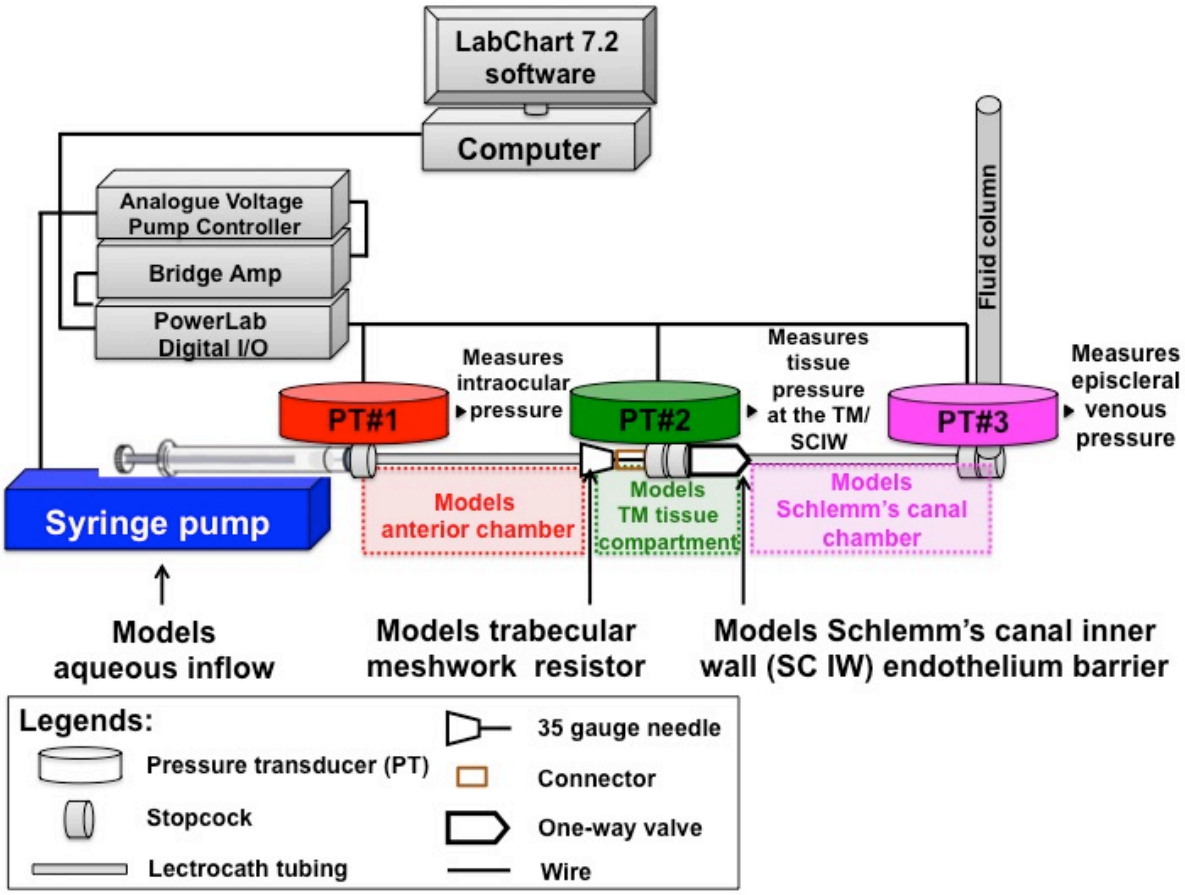

Figure 1. Schematic diagram of the experimental setup of the artificial perfusion model. This model had the following components: 1) A 50µl microsyringe driven by a microsyringe pump simulating aqueous production; 2) 35G needle representing TM resistor; 3) one-way valve representing SC IW barrier; and 4) distal fluid column that allows variable fluid height generating EVP. All were connected in series via rigid tubings (Lectrocath). Three intervening PTs recorded pressures corresponding to different fluid compartments of the eye: a) PT#1 in fluid compartment between the microsyringe pump and needle measured pressure in the artificial anterior chamber (measuring simulated IOP); b) PT#2 between the needle and valve provided proxy pressure measurement at the TM/SC IW tissue interface (measuring simulated tissue compartment pressure); and c) PT#3 between the valve and column (measuring simulated EVP). The microsyringe pump was connected to an analogue voltage controller, bridge amplifier and digital input/output (I/O), providing a feedback loop to allow perfusion at a predetermined constant pressure or flow rate. Moment-to-moment pressure and flow rate were simultaneously sampled at millisecond intervals and viewed in real time on LabChart analytical software.

2.1.2 Pressure transduction

Various fluid chambers were connected in series via noncompliant, rigid tubes (Lectrocath tube, 1mm internal diameter, 15cm length; Vygon Corporation, Montgomeryville, PA). Intervening pressure transducers (PT; P75, Hugo Sachs, March–Hugstetten, Germany) recorded pressures in the fluid chambers corresponding to the various fluid compartments of the aqueous drainage route: (1) PT#1 between microsyringe pump and needle measured pressure in the artificial anterior chamber (representing IOP); (2) PT#2 between needle and valve measured pressure between a needle and one-way valve (simulating pressure in the TM/SC IW tissue interface or tissue compartment pressure); and (3) PT#3 measured pressure in the SC chamber between valve and distal column, simulating SC pressure (taken here to be EVP).

Each PT was attached to its own 3-way stopcock with a male non-vented cap (Edwards Lifesciences, Irvine, CA). PT#2 had a further stopcock to allow characterization of needle resistance. A polypropylene female-to-female connector (Harvard apparatus, Holliston, MA) secured by luer lock proximal to the PT#2 stopcock was glued in a water-tight fashion to the distal part of the 35G needle. PT#3 also had a second stopcock to allow attachment of a fluid column to provide hydrostatic pressure to generate EVP (as described earlier). Additional fluid columns were used to calibrate PT and verify pressure readings. Prior to starting experiments, the system was calibrated and zero-referenced, and unit conversion confirmed. All components of the artificial perfusion system and tubings were filled and primed with Dulbecco's Phosphate Buffered Saline (DPBS; Mediatech, Corning, Manassas, VA)

to exclude air bubbles. The system was also meticulously scrutinized to ensure absence of air bubbles.

2.1.3 Electronics and data handling

The microsyringe pump was connected to an analogue voltage controller (STH Pump Controller; AD Instruments), which was connected to a bridge amplifier (Octal Bridge Amp; AD Instruments, Colorado Springs, CO) and subsequently to a digital I/O interface that recorded, displayed and allowed data analysis (Powerlab; AD Instruments, Colorado Springs, CO) in LabChart software (Version 7.2, ADInstruments, Colorado Springs, CO) on a computer.

The pump was rated by the manufacturer to deliver flow rates ranging from 0.1nl/h to 220ml/min with accuracy within 0.35% and reproducibility within 0.05% (PhD Ultra datasheet). The voltage controller received feedback from the pump, PTs and bridge amplifier for real-time feedback control to allow either constant pressure or constant flow perfusion (see below).

Pressure (measured by PTs) and flow rate (from the pump) were simultaneously sampled at 10 millisecond intervals for 2 minutes or 12,000 consecutive data points and viewed using the software. To allow for pump stabilization, data from the first minute (first 6,000 consecutive data points after changing flow or pressure perfusion settings) were discarded. The second 6,000 consecutive data (or the second minute of the experiment) from each pressure or flow rate setting changed were used for analysis.

2.1.4 Perfusion protocols

2.1.4.1 Constant pressure and constant flow perfusion

The setup permitted perfusion by constant pressure or constant flow: (1) constant pressure perfusion was used to examine aqueous dynamics at a predetermined IOP. Constant pressure in the anterior chamber (PT#1; IOP) was achieved with a previously described voltage feedback system[68] that automatically varied flow rate to maintain a constant preset pressure. The transduced pressure was always monitored and compared by the controller with a predetermined set-point pressure value. Based on the difference between the transduced and set-point pressure, the integrator would used this data to adjust the pump accordingly (i.e., the pump slowed down if the transduced pressure was too high and vice versa).[69] (2) Constant flow perfusion was conducted to examine aqueous dynamics over a period of steady state aqueous flow (production). This was achieved by presetting the pump flow rate without automatic feedback control, during which voltage output to the pump was manually preset at eight different settings to determine flow rate. All measurements at constant pressure or constant flow perfusion were performed in triplicate.

2.1.4.2 Variability of pressure during constant pressure perfusion

The coefficient of variation (CV) of pressure during constant pressure perfusion at different preset pressures over time was analyzed to assess the model's ability to maintain pressure. CV was calculated by dividing the standard deviation over mean at each pressure setting, which was collected every 10 milliseconds during sequential 15 second blocks (1,500 measures per 15 second block) over 120

seconds based on triplicate measurements. This data was used to determine the variability of the system in how it quickly stabilized to a new pressure set point.

2.1.4.3 Needle resistance

Resistance of the 35G needle was used to simulate TM resistance to aqueous outflow. To measure resistance, the needle was isolated before conducting constant flow perfusion at eight different flow rates as described earlier under 2.1.4.1. Pressure transduced at different flow rates was recorded. Needle resistance (representing TM resistance) was calculated from the slope of the PT#1 pressure (mmHg) versus flow rate (µl/min) function plotted (by scatter plots) and modeled using regression analysis. Statistical analysis was done in Excel® 2011 for Mac (Microsoft, Redmond, WA). During perfusion, the tip of the needle was submerged in DPBS.

2.1.4.4 One-way valve

A one-way valve mimicking the SC IW endothelium barrier allowed a pressure differential to be maintained between the anterior chamber and tissue compartment from the SC chamber. The integrity of the one-way valve was verified in the artificial perfusion system before each experiment. Stopcocks were opened to allow fluid to flow from the distal fluid column to the SC chamber until fluid reaches the valve. A valve was accepted as functional if characteristic pressure tracings from all PTs confirmed maintenance of a pressure differential between the tissue compartment and SC chamber (i.e., no retrograde flow; see later in Figure 9B).

Valve resistance represented the contribution of simulated SC IW endothelium to outflow resistance. This was determined indirectly by calculating the difference between resistance measured from the whole artificial perfusion system (including needle and valve) and resistance of the perfusion system connected only to the needle (i.e. same system but with value omitted). Combined resistance from the needle and valve in series represented total simulated outflow resistance in the conventional outflow model.

2.1.4.5 Outflow facility

Outflow facility could be determined by constant pressure or constant flow perfusion. During constant pressure perfusion, after achieving steady state pressure, stable pressure transduction at PT#1 for at least two minutes at each pressure setting was recorded at a series of preset pressures. Data from the second minute was used to determine outflow facility as data from the first minute was discarded to allow for stabilization. Outflow facility was determined using the slope of flow rate (µl/min) versus pressure (mmHg) function plotted (by scatter plots) and modeled using regression analysis. Statistical analysis was also done in Excel® 2011 for Mac (Microsoft, Redmond, WA).

2.2 Simulation of conventional aqueous outflow dynamics under pathological conditions from an artificial hydraulic model

The setup simulating pathological scenarios of the aqueous outflow dynamics in the conventional pathway was almost similar to the setup under physiological conditions. Differences between these two setups include a (1) 35G needle, which was modified by gently clamping with a pair of pliers to achieve a smaller bore diameter simulating a TM resistor with elevated resistance; (2) higher fluid height in the distal fluid column replicated elevated EVP, which allowed the system to attain two levels of EVP (one at 11mmHg and the other at 15mmHg). These two changes in the artificial perfusion system simulated pathological scenarios associated with the conventional outflow pathway leading to elevated IOP. Increase in needle resistance simulated glaucoma with increased TM resistance while the higher fluid height in the column replicated secondary glaucoma due to elevated EVP. Care was taken to avoid excessive force when clamping the 35G needle. Once modified, the needle resistance was measured and the same needle was used throughout the study. Dynamics between PT#1 (IOP), PT#3 (EVP) and onset of outflow were obtained and compared under both physiological and pathological conditions.

Chapter 3: Empirical insights into conventional outflow dynamics from an artificial hydraulic model

The work associated with results and discussion of Chapter 3 was presented at the Association for Research in Vision and Ophthalmology Annual Meeting 2013 at Seattle, USA[70] and currently being prepared for submission as a paper for a journal article.

3.1 Results

3.1.1 Determination of pressure stability at different preset pressure settings using constant pressure perfusion

Constant pressure perfusion maintains consistent pressure at PT#1 pressure (IOP) by automatically varying flow rate. A representative tracing demonstrated gradual increasing pressures from 6mmHg to 15mmHg that reached steady-state almost immediately and maintained over time (as shown in Figure 2A) with its corresponding flow rates (as shown in Figure 2B). Based on triplicate measurements, the average CV of pressure over time was 0.6%, and in every preset pressure setting, CV was either 0.01 or less.

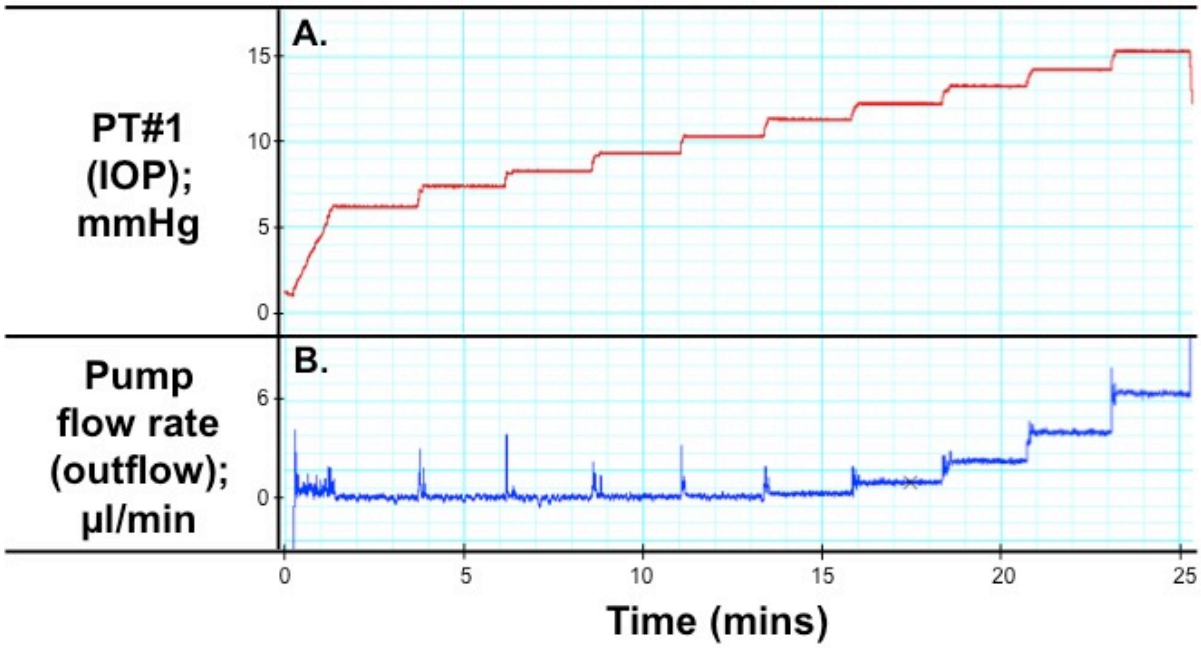

Figure 2. Representative tracing of pressure **(A)** and its corresponding flow rate **(B)** using constant pressure perfusion. **A.** Demonstrates how steady-state pressure was achieved almost immediately with change in pressure setting (from 6-15mmHg) and was maintained over time. **B.** Illustrated tracing spikes as a temporary increase in flow rate as the pump compensated by speeding up to reach the new steady-state pressure setting.

3.1.2 Contribution of TM (needle) and SC IW (one-way valve) to outflow resistance in the model

The following resistances were measured: model with needle resistor only (representing TM; Figure 3A), and model combining needle and valve (representing TM + SC IW respectively; Figure 3B). Pressure versus flow functions were linear, yielding regression models of $y=0.57x-0.02$ ($R^2=1.00$) for the model with needle only (Figure 3A) and $y=0.62x+11.03$ ($R^2=1.00$) for a model combining needle and valve (Figure 3B). Pressure (PT#1) was higher by an average of 11.14mgHg during perfusion through the model in the combined needle and valve compared with the model with needle only, likely reflecting a combination of the valve's intrinsic flow-through resistance and opening pressure (pressure at which the valve opens). Based

on regression models, combined 35G needle-valve resistance was 0.62mmHg/µl/min; 35G needle resistance was 0.57mmHg/µl/min, marginally less then combined 35G needle-valve resistance by 0.05mmHg (8.1%). Thus, the separate outflow resistances originating from the simulated TM (needle) and SC IW (valve) contribute to total outflow resistance in the model.

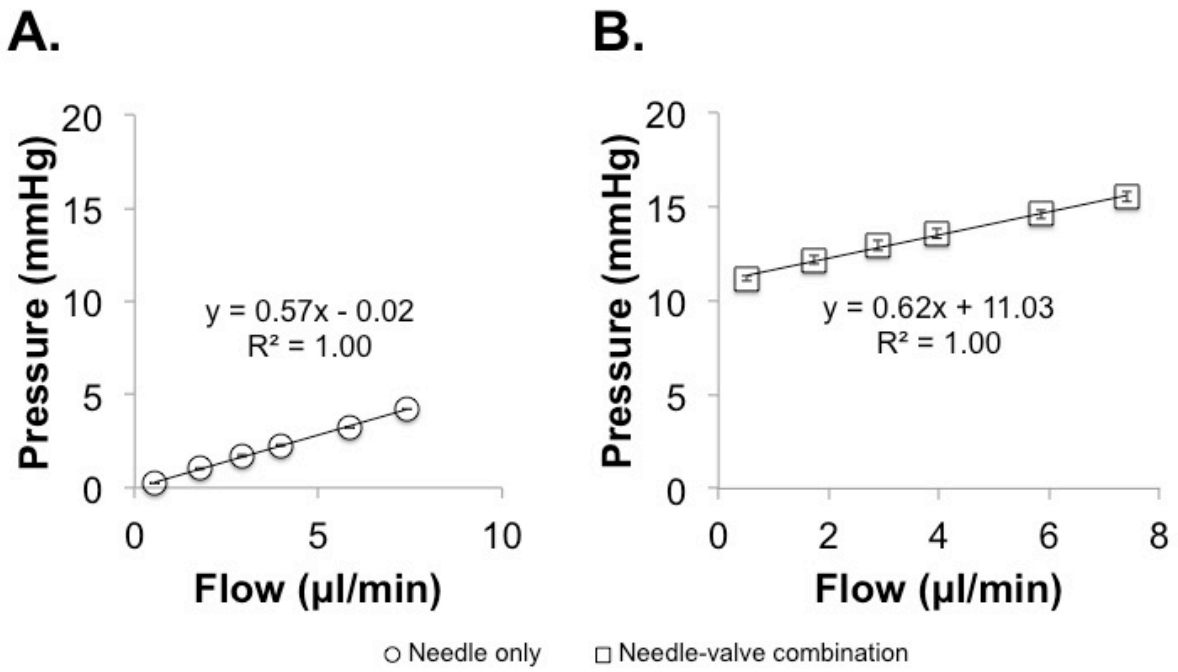

Figure 3. Pressure-flow relationships reflecting resistance in the model containing needle resistor only (**A**; representing TM), and combined needle and valve (**B**; representing TM and SC IW respectively). Addition of the valve (SC IW) in the presence of the needle (TM) increased outflow resistance by 8.1%, yielding pressure (PT#1; IOP) that was 11.14mmHg higher on average compared with a scenario wherein the model had a needle but no valve. Error bars: standard error of mean (SEM) based on triplicate measurements.

3.1.3 Outflow starts when IOP exceeds EVP

Under feedback-controlled constant pressure perfusion, outflow in the apparatus was zero and the pump did not start until PT#1 (IOP) pressure was raised to exceed PT#3 (EVP; set at 11.8mmHg in the model), as shown in Figure 4A. At pressures (PT#1; IOP) above PT#3 (EVP=11.8mmHg), pump flow rate (representing outflow rate under constant pressure perfusion) was pressure-dependent, increasing linearly with PT#1 (IOP), as depicted in Figure 4B.

Thus in a model pre-set to a constant pressure, resistance provided by the needle allowed PT#1 (IOP) pressure to exceed a value of PT#3 (EVP), and for IOP to be maintained over EVP. Without needle resistance (see later in Figure 6), a surge of unimpeded outflow occurred when PT#1 (IOP) pressure exceeded PT#3 (EVP), causing difficulty in maintaining pressures in both PT#1 (IOP; anterior chamber) and PT#2 (TM/SC IW compartment pressure).

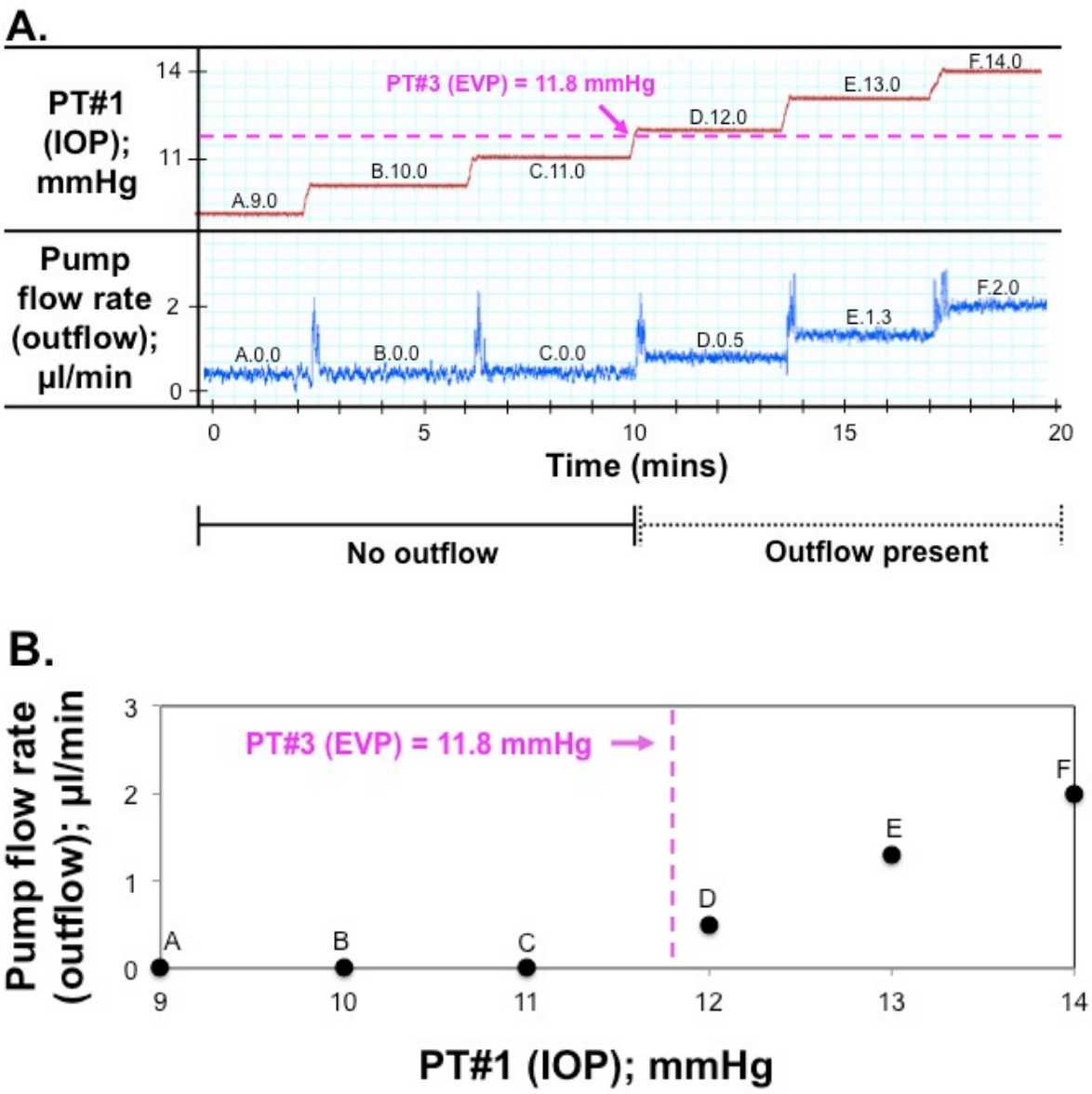

Figure 4. A. Representative tracings showing that outflow (lower trace) starts when IOP (upper trace; PT#1) exceeds EVP (pink dotted line: 11.8mmHg; PT#3). Below this level, outflow is zero (9-11mmHg). Above this level, outflow increases with IOP (12-14mmHg). **B.** Data plot of the relationship between pump flow rate (outflow) and PT#1 pressure (IOP) wherein a linear increase in outflow rate occurs once the PT#3 (EVP) level is exceeded.

3.1.4 Outflow stops when EVP exceeds IOP

Pump flow rate remained zero until PT#1 pressure (IOP; 12.7mmHg) increased to exceed PT#3 (EVP; 11.6mmHg), as shown in Figures 5A and 5B. When PT#3 (EVP; 15.4mmHg) was raised to exceed PT#1 pressure (IOP; 13.7mmHg), the pump stopped, as did outflow also shown in Figures 5A and 5B. Hence, outflow stops when EVP rises to exceed IOP, and by implication, a compensatory rise in IOP to exceed the higher EVP must occur to restore outflow.

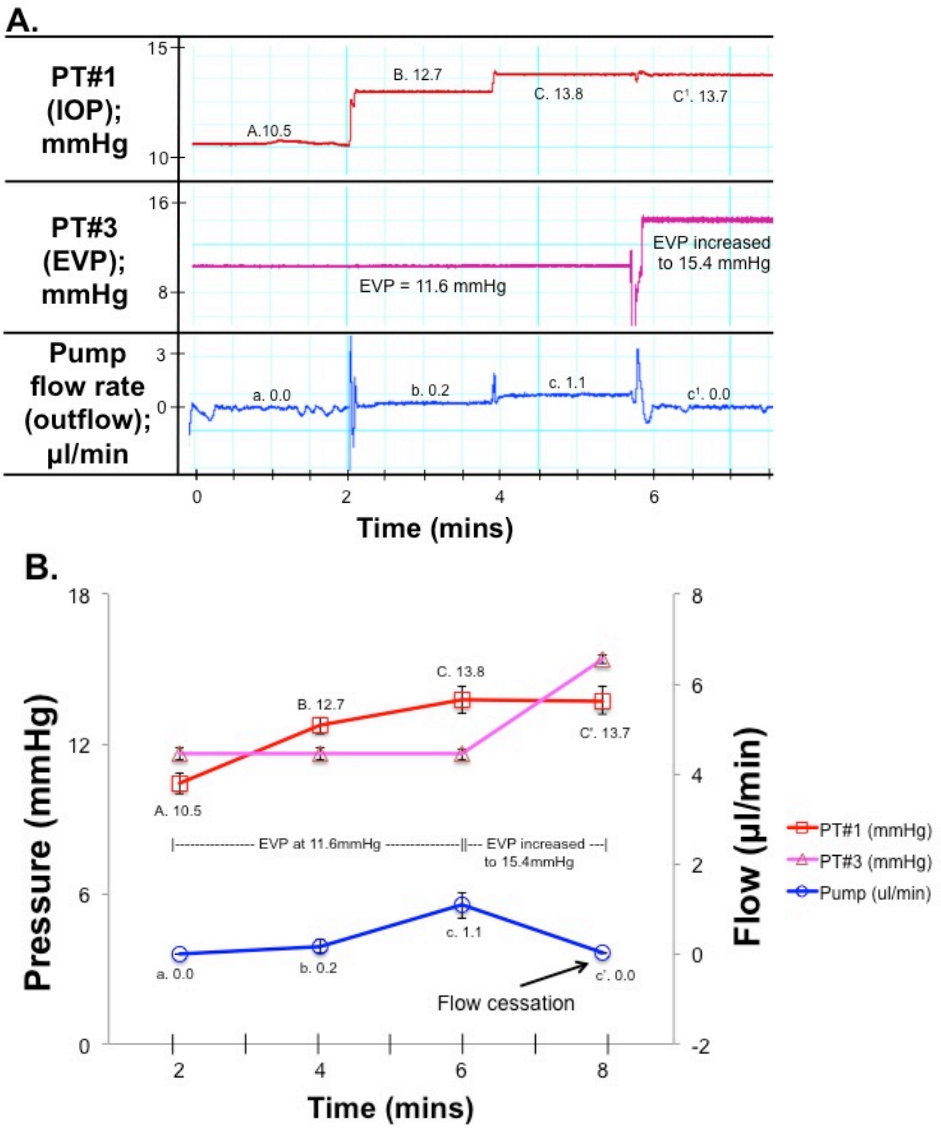

Figure 5. A. Representative tracings illustrating that outflow starts when pressure in PT#1 pressure (IOP) exceeds PT#3 (EVP). The pump stopped (flow rate zero) when PT#3 (EVP) was raised above PT#1 pressure (IOP). **B.** Data plots showing relationships between PT#1 (IOP), PT#3 (EVP) and pump flow rate over time. Error bars (SEM) based on triplicate measurements.

3.1.5 IOP-EVP pressure gradient and pressure-dependent outflow are not sustainable without an outflow resistor once PT#1 (IOP) exceeds PT#3 (EVP)

In the absence of a needle resistor (representing TM), with PT#1 (IOP) and PT#2 pressures (tissue compartment pressure) below EVP, and with no outflow (zero pump flow rate), PT#1 and PT#2 pressures were equal, as shown in Figure 6. However, when PT#1 and PT#2 pressures exceeded EVP, unrestricted outflow occurred and PT#1 and PT#2 pressures could not be maintained, leading to precipitous drops in simulated IOP and tissue compartment pressure (also seen in Figure 6). Thus, in the absence of TM resistance, maintenance of (a) a pressure gradient between anterior chamber and SC, and (b) pressure-dependent outflow were not possible for IOP levels above EVP.

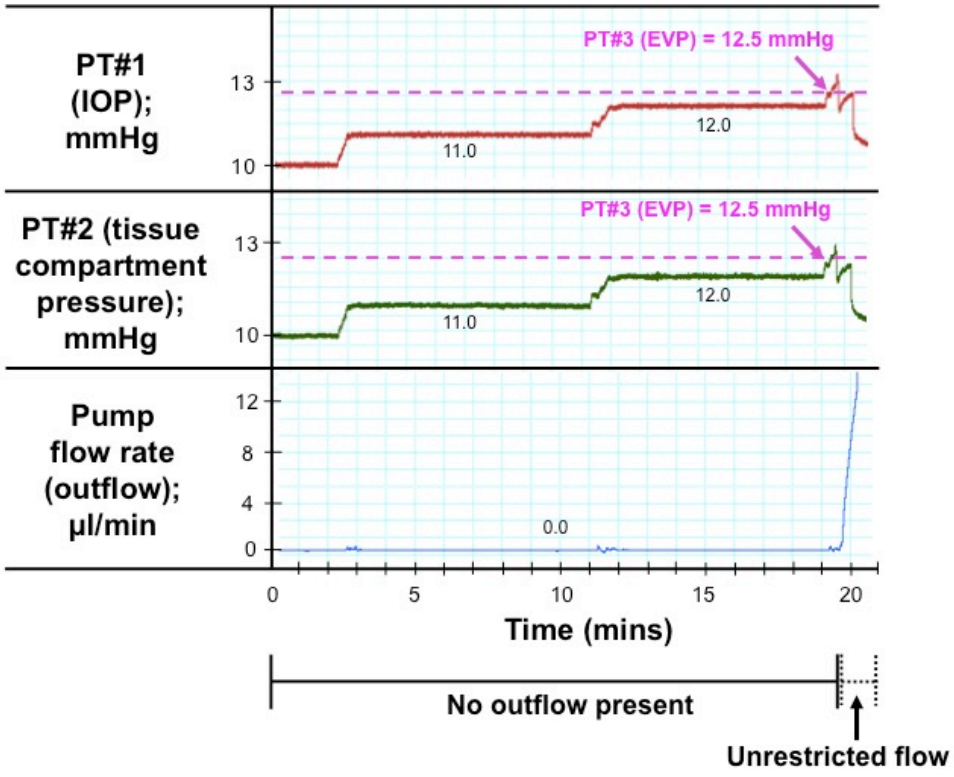

Figure 6. Representative traces showing that without an outflow resistor, the PT#1-PT#3 (IOP-EVP) pressure gradient and pressure-dependent outflow could not be maintained once PT#1 (IOP)>PT#3 (EVP).

3.1.6 Outflow resistor allows sustained pressure-dependent outflow

In the presence of an outflow resistor (35G needle, representing TM), outflow commenced when PT#1 pressure (IOP) exceeded PT#3 (EVP), as shown in Figure 7A. For PT#1 (IOP) values over PT#3 (EVP), the outflow rate increased with PT#1 pressure and was sustained at each pressure setting over time in the presence of the needle resistor. Thus, TM resistance permits sustained pressure-dependent outflow at IOP levels above EVP.

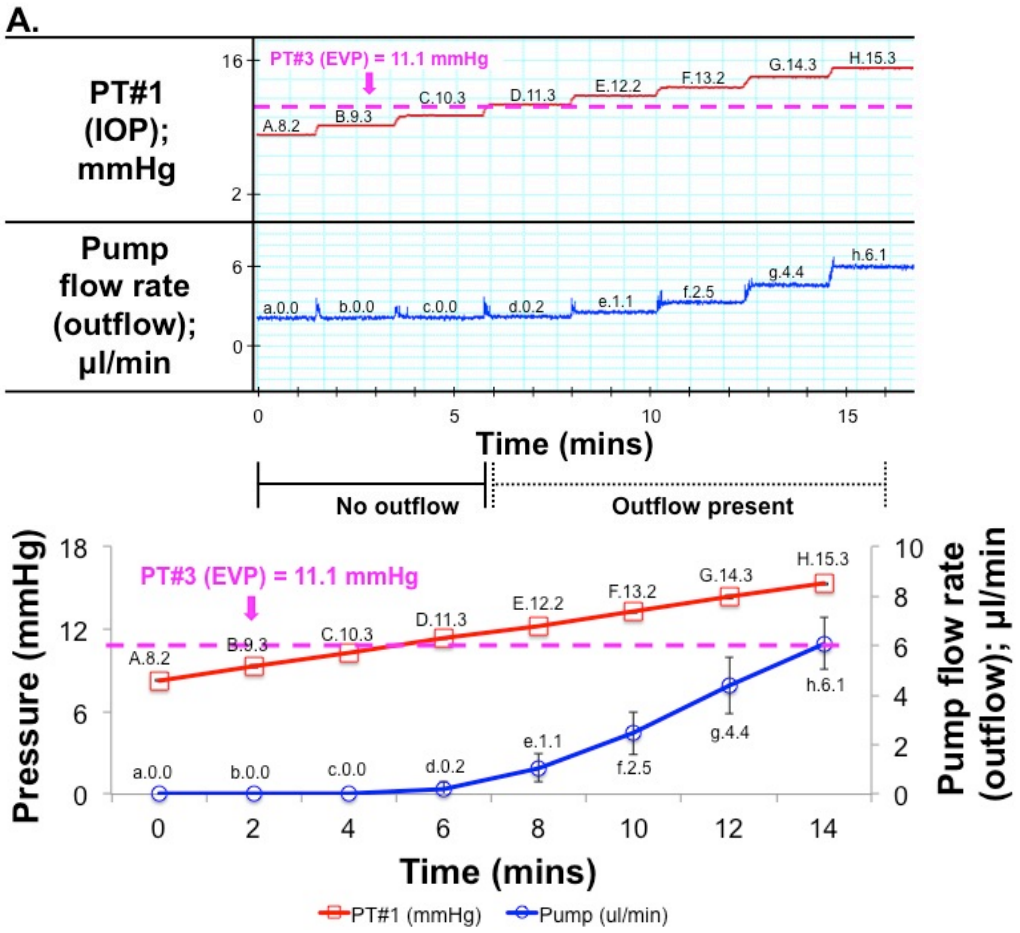

Figure 7. An outflow resistor is needed to maintain a pressure gradient between PT#1 (IOP) and PT#3 (EVP) and pressure-dependent outflow for PT#1 pressures above PT#3. **A.** Representative tracings (top) and data plots (bottom) for PT#1 pressure and pump flow rate (outflow) over time with reference to PT#3. Data plots and error bars (SEM) were based on triplicate measurements. In the presence of an outflow resistor, the constant pressure set point for PT#1 was increased from 8.2mmg to 15.3mmHg. The pump started when PT#1>PT#3 (EVP set at 11.1mmHg) and thereafter flow rate increased with PT#1. Data plots reveal a pattern of increasing flow rate with increasing PT#1 pressure once PT#1>PT#3. Flow rate was zero when PT#1<PT#3.

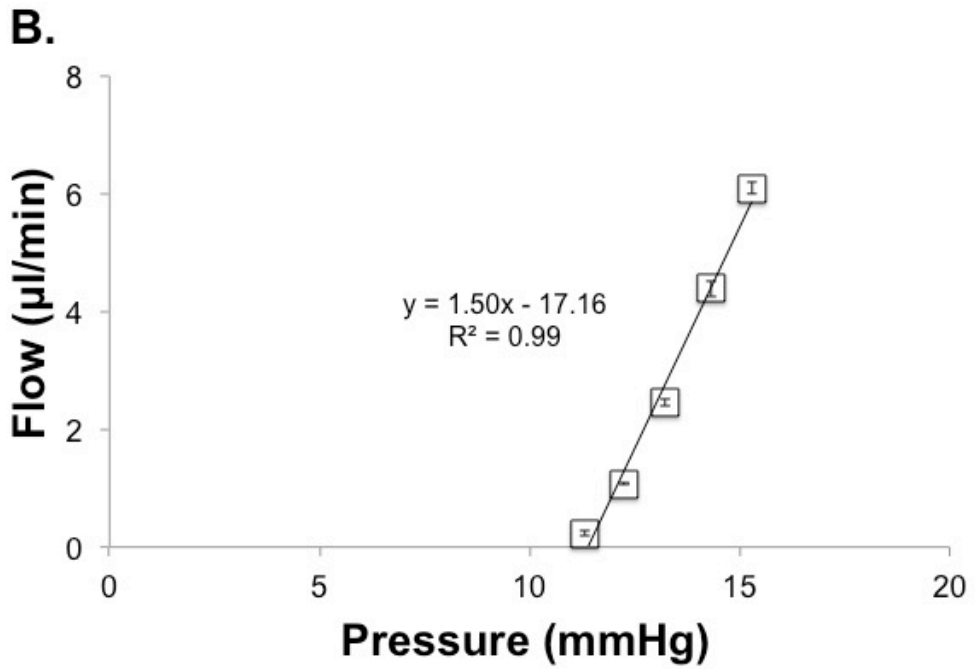

Figure 7B. In the presence of a needle resistor, a linear relationship was seen between flow and pressure (PT#1) for PT#1>PT#3, as described by a regression model of y=1.50x-17.16 (R^2=0.99). Data points and error bars (SEM) were based on triplicate measurements.

3.1.7 Outflow resistor allows establishment of pressure gradient across the TM

In the presence of an outflow resistor (35G needle, representing TM), pump flow (outflow) commenced when pre-set PT#1 pressure (IOP) exceeded PT#3 (EVP). With outflow above zero, a pressure differential emerged between PT#1 (IOP) and PT#2 (tissue compartment pressure), as shown in Figure 8A. The PT#1-PT#2 pressure differential was sustained over time for an outflow rate. When PT#1>PT#3 (i.e., IOP>EVP), the PT#1-PT#2 pressure differential starts to increased with greater flow rate (Figure 8C) and divergence of PT#1 and PT#2 pressures was seen due to different resistances across the needle (TM) and valve (SC IW), as shown in Figure 8B. Thus, for IOP>EVP, TM resistance allows separate pressure gradients across

the TM and SC IW to be established. Pressure gradients across the TM and SC IW vary with IOP and outflow.

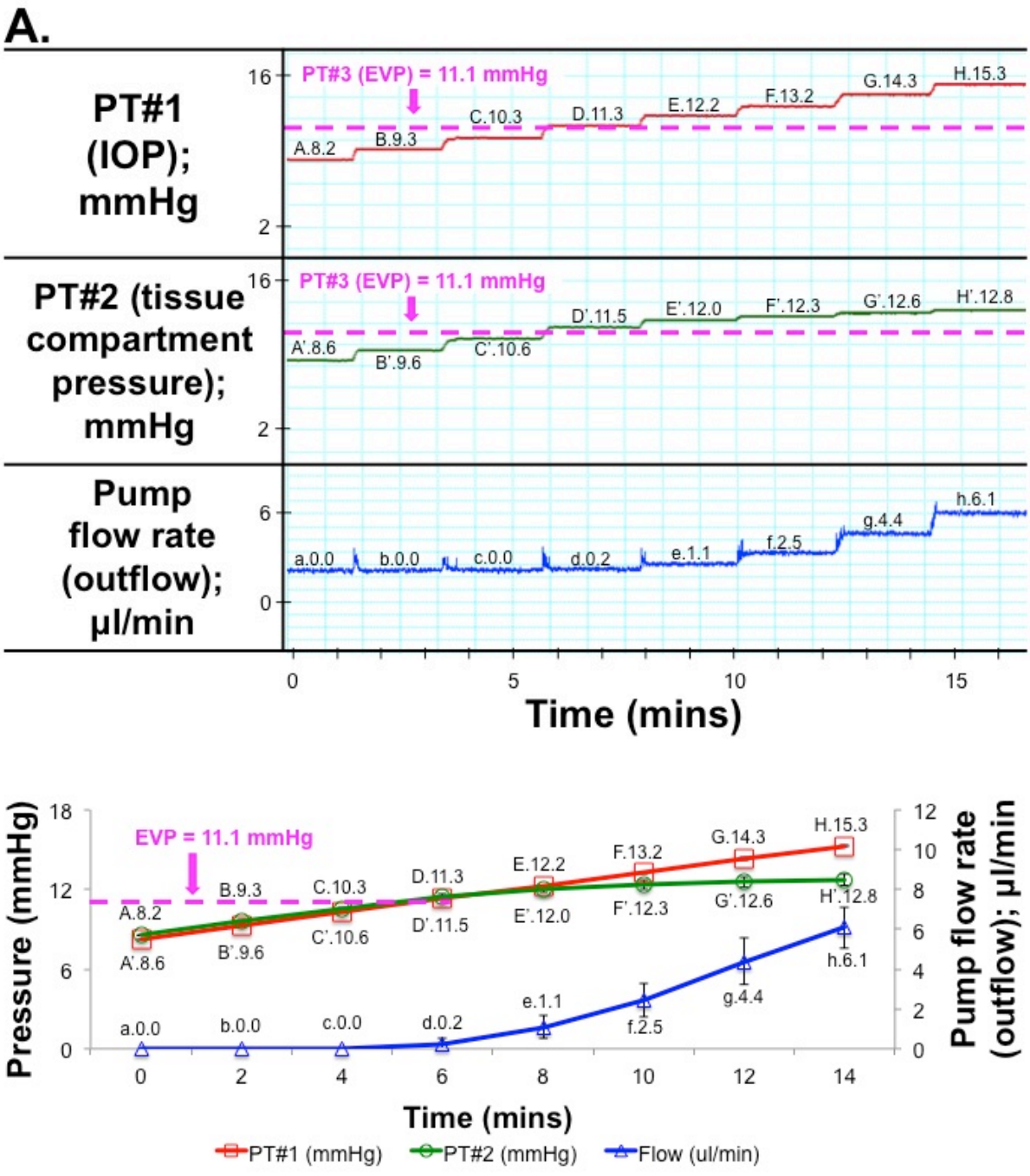

Figure 8. In the presence of an outflow resistor (TM) and PT#1>PT#3 (IOP>EVP), a sustained PT#1-PT#2 (trans-TM) pressure differential is established that increases with PT#1 pressure (IOP) and pump flow rate (outflow). **A.** Representative traces (top) and data plots (bottom) for PT#1, PT#2 and pump flow rate (outflow) over time with reference to PT#3. Data plots and error bars (SEM) were based on triplicate measurements.

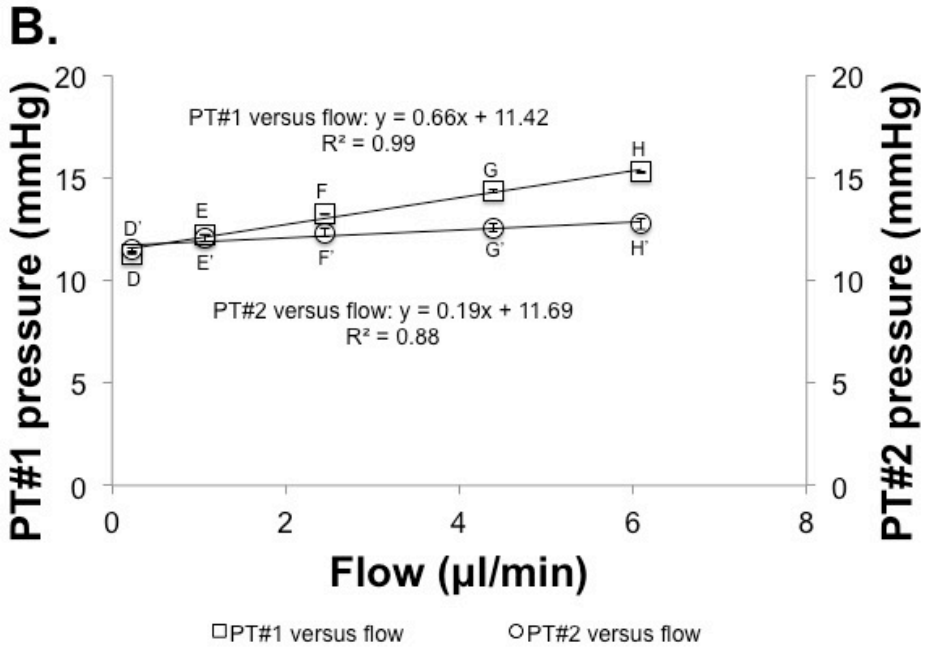

Figure 8B. Data plots of pressure-flow relationships for PT#1 (left) and PT#2 (right) with slopes of linear regression models representing needle (y=0.66x+11.42; R^2=0.99) and valve (y=0.19x+11.69; R^2=0.88) resistance, respectively. Markers D to H and D' to H' corresponded to the markers seen in Figure 8A (top and bottom) that coincided in the presence of flow when IOP>EVP during constant pressure perfusion. Data plots and error bars (SEM) were based on triplicate measurements.

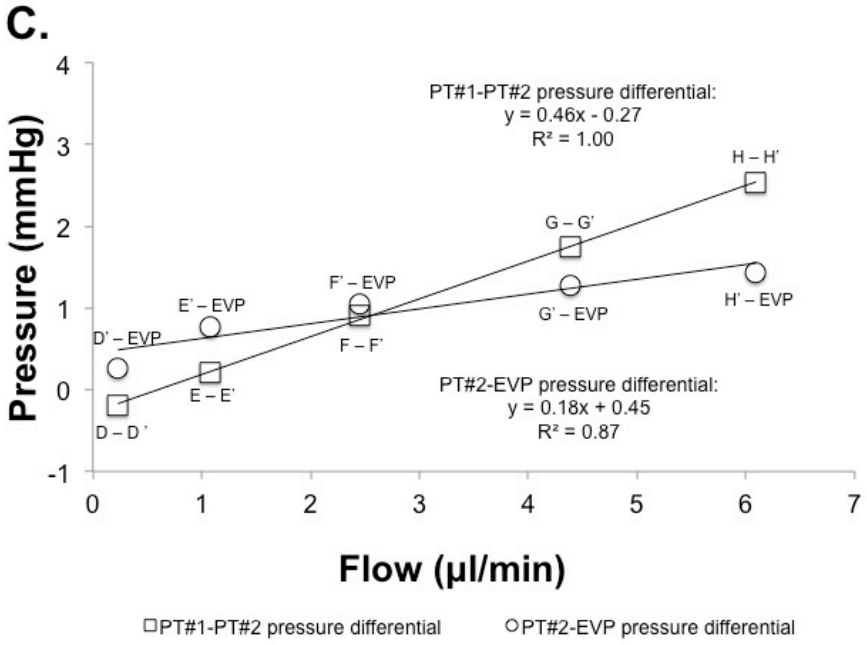

Figure 8C. Data plots showing the relationship between PT#1-PT#2 and PT#2-EVP pressure differentials and flow rate (outflow) reflecting resistance in the TM needle resistor was greater than the valve (SC IW). Linear regression models for PT#1-PT#2 pressure differential and PT#2-EVP pressure differential were y=0.46x-0.27 (R^2=1.00) and y=0.18x+0.45 (R^2=0.87), respectively. Data plots and error bars (SEM) were based on triplicate measurements.

3.1.8 Pressure differential between anterior chamber and SC was established by a one-way valve

The one-way valve prevented retrograde flow from the SC chamber to anterior chamber. This was demonstrated by filling the fluid column with DPBS to a height corresponding to a pre-set pressure measured by PT#3 (EVP) with the stopcock connected to the fluid column shut off from the rest of the perfusion system. Upon opening of the stopcock (black arrow) between the column and SC chamber, measured pressure in PT#3 rose immediately, as shown in Figures 9A and 9B. In the absence of the one-way valve, pressure equilibrated across all compartments as measured by PT#1-3 when the stopcock of the fluid column was opened (black arrow), as shown in Figure 9A. In the presence of a one-way valve, a pressure differential was established between (a) PT#3 (8.0mmHg) and PT#1 (IOP; 0.5mmHg), and between (b) PT#3 (8.0mmHg) and PT#2 (0.5mmHg), as shown in Figure 9B. In Figure 9C, when PT#1 pressure (IOP; 12.5mmHg) exceeded PT#3 (EVP; 11.5mmHg) and pump flow commenced, the pressure differential between PT#1 and PT#2 widened. Thus, the one-way flow valve-like characteristic of SCIW allows development of a pressure differential between IOP and EVP and establishes pressure gradients across TM and SC IW.

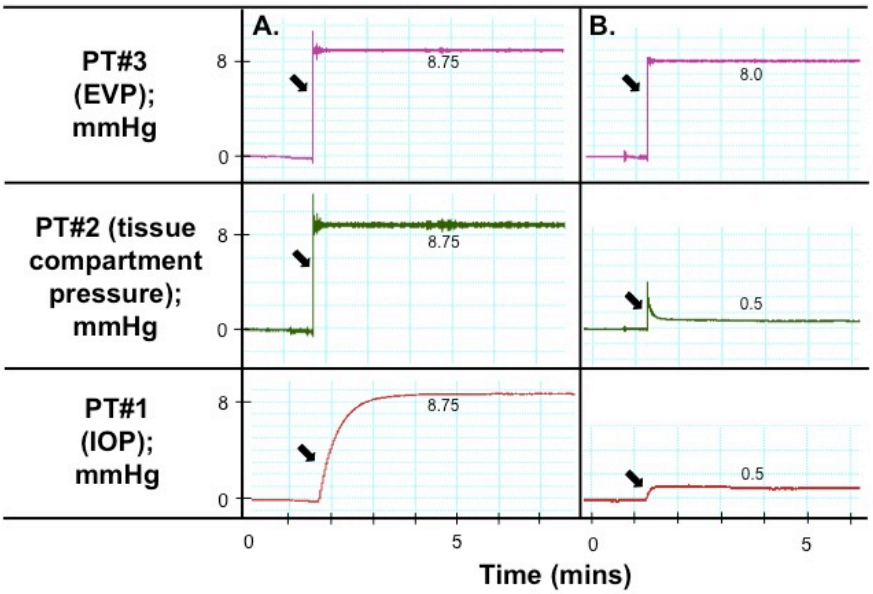

Figure 9. A one-way valve allows pressure differentials to develop between the anterior chamber and SC. **A.** Representative trace in the absence of a one-way valve. Immediate equilibration of pressure across all compartments (PT#1-3; all 8.75mmHg) occurred after the stopcock to the distal fluid column was opened (black arrow). **B.** In the presence of a one-way valve, a pressure differential was established between (i) PT#3 and PT#1, and (ii) PT#3 and PT#2 when the stopcock to the distal fluid column was opened (black arrow).

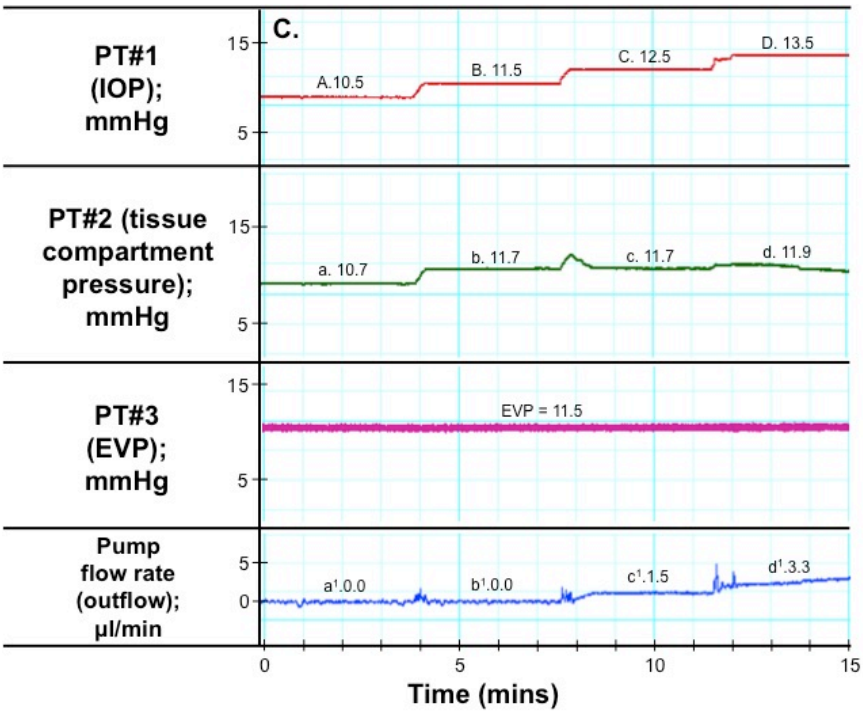

Figure 9C. With outflow established once PT#1 pressure (IOP; 12.5mmHg) exceeded PT#3 (EVP; 11.5mmHg) under constant pressure perfusion in the presence of a needle resistor and one-way valve, a pressure gradient between PT#1 (IOP) and PT#2 (tissue compartment pressure) from PT#3 (EVP) developed. As PT#1 pressure (IOP) continued to rise above PT#3 (EVP) and flow rate increased, the pressure gradient between PT#1 and PT#2 also increased.

3.1.9 Constant flow perfusion yields a constant pressure when IOP was above EVP

At a constant pump flow rate (inflow) with PT#1 (IOP) < PT#3 (EVP), PT#1 pressure increased linearly until PT#3 pressure was reached, as shown in Figure 10A. Once PT#1>PT#3, the constant pump flow rate (inflow=outflow) yielded a constant PT#1 pressure (IOP) that changed with flow rate. Thus, aqueous inflow at a constant rate yields a constant IOP when IOP is above EVP, with the rate of IOP increase per unit of flow rate determined by outflow resistance.

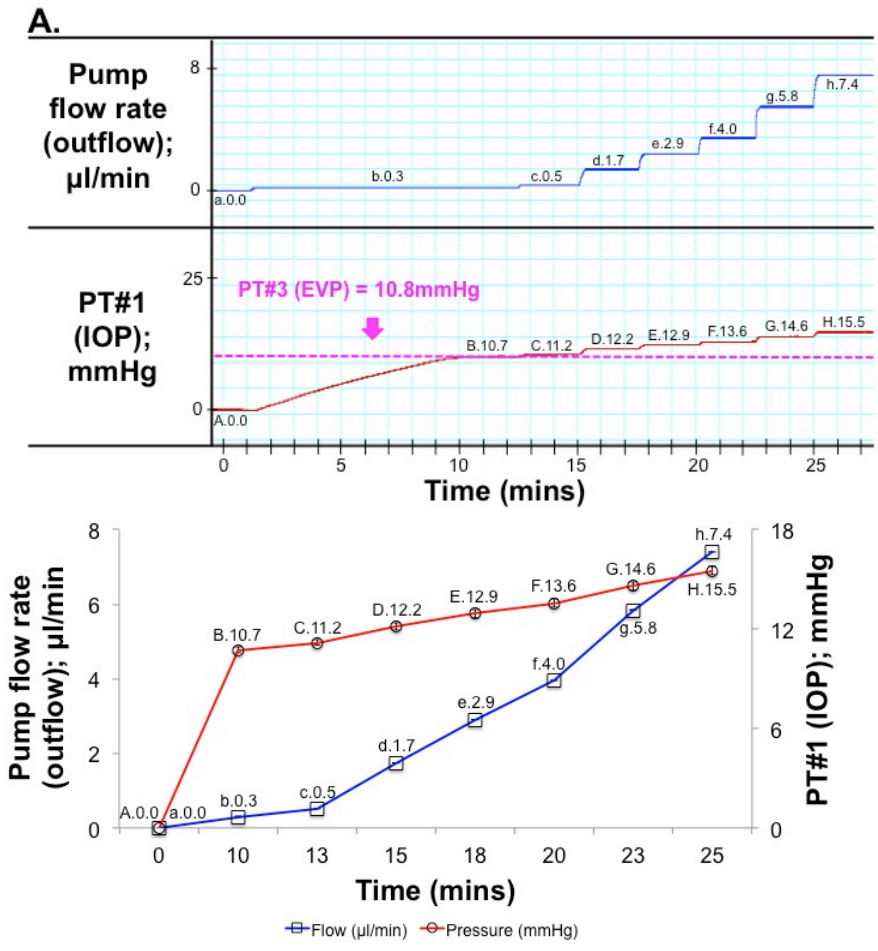

Figure 10. Relationship between pump constant flow rate (inflow/outflow), PT#1 (IOP) and PT#3 (EVP) over time. **A.** Representative tracings (top) showing that with perfusion at a constant flow rate, PT#1 pressure (IOP) increased linearly until PT#3 (EVP) was exceeded, after which PT#1 remained unchanged at a constant flow rate. Data plots (bottom) showing relationship between pump flow rate (outflow) and PT#1 pressure (IOP) over time based on triplicate measurements. Data plots and error bars (SEM) were based on triplicate measurements.

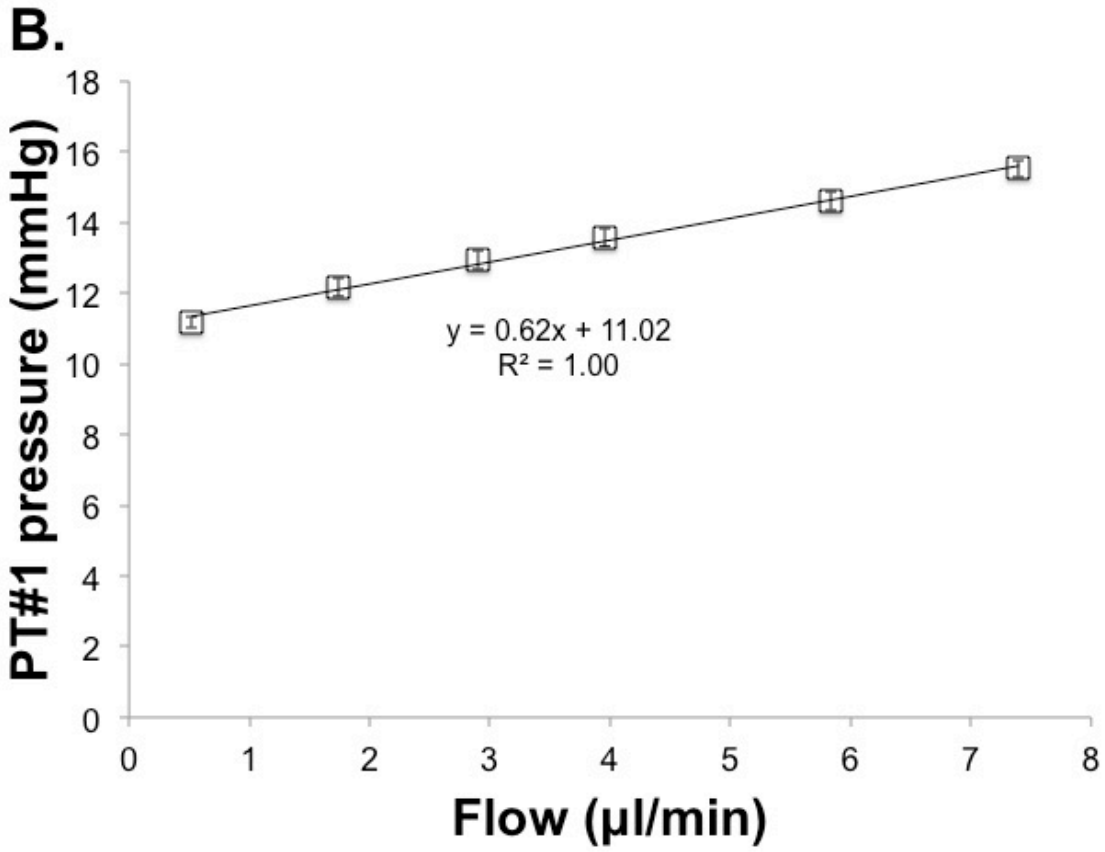

Figure 10B. Data plot of relationship between PT#1 pressure (IOP) and flow rate for PT#1>PT#3 showing a linear regression model of y = 0.62x+11.02 (R^2=1.00). The slope representing total outflow resistance was similar as measured during constant pressure perfusion.

3.1.10 Summary of results from simulation of the conventional outflow pathway under physiological conditions

Observation of important points are enumerated as follows:

- Total outflow resistance was contributed by two components: 35G needle simulating the TM and the one-way valve simulating the SC IW. The needle resistor had a higher outflow resistance compared to the valve.

- The relationship between IOP and EVP determined the onset and cessation of outflow. Outflow started as PT#1 (IOP) reached and exceeded EVP (PT#3). However, outflow stopped when EVP rose above IOP.

- The 35G needle (outflow resistor) was responsible for the following observations: 1) maintaining IOP-EVP pressure gradient as well as pressure-dependent outflow; and 2) establishment of a pressure-gradient between the TM and SC IW (in the presence of outflow).

- The one-way valve provided the pressure differential between the simulated anterior chamber and SC. In the absence of the valve, equilibration of pressure across all fluid compartments occurred upon opening of the stopcock connected to the fluid column.

- IOP linearly rose to the level of EVP with constant aqueous inflow. Once IOP reached EVP, constant flow rate ensued generating a constant IOP as determined by outflow resistance.

3.2 Discussion

Empircal insights into the conventional aqueous outflow dynamics were provided by an artificial hydraulic model of the conventional drainage system incorporating the following key components: (1) variable fluid flow rate to mimic aqueous inflow at a constant rate or to generate a constant IOP regulated by a pressure-flow feedback loop; an anterior chamber; TM outflow resistance using a

35G needle; SC IW barrier with its own intrinsic outflow resistance and one-way outflow without retrograde flow using a one-way valve; outflow through SCIW into SC; and EVP that was separately generated by a distal hydrostatic system. There was capacity to measure pressure in the anterior chamber (IOP); TM-SC IW tissue interface (TM tissue compartment pressure); and SC (representing EVP); and by knowing the outflow rate, the different resistances of TM and SC IW could be determined.

Based on pressure-flow tracing as shown in Figures 2A & 2B, pressure at steady-state was immediately reached (at least within one minute) with each change in pressure setting. Stability to maintain pressure was validated by calculating the average CV of all pressure settings (from 6-15mmHg) over time, which was 0.6%, indicative of minimal variability.

The model correctly and empirically predicts that conventional outflow occurs only when IOP exceeds EVP both in scenarios where IOP and aqueous inflow are constant. To ensure continuous outflow at a constant steady-state IOP, it is essential to be able to sustain IOP above EVP. An outflow resistor allows for this controlled dynamic. Without the resistor, unrestrained outflow would ensue whenever the eye seeks to establish a constant IOP over EVP. The TM was assigned the role of primary resistor in the model but this could easily be assigned to the SC IW as there is currently some unresolved debate[12-19,45] on which tissue predominates as a resistor. Once IOP is established at a level over EVP, EVP may itself rise over time to exceed IOP as occurs in some diseases with elevated EVP causing secondary glaucoma. With constant aqueous inflow, IOP would again reestablish itself above

EVP, even at a higher pressure that corresponded in maintaining outflow under higher EVP. Here, the higher IOP would be due to excessive EVP rather than excessive outflow resistance.

Conventional outflow is driven by a pressure gradient from the anterior chamber (IOP) to SC (EVP), as predicted by the classic Goldman equation. This hydraulic model provided capacity to further resolve contributions of the trans-TM and trans-SC IW pressure gradients to outflow. It is technically difficult to measure proportionate resistance across regions of the drainage tissue *in vivo* or *in situ*, but this was possible in our model due to the separation of TM resistor and SC IW valve combined with placement of an intervening pressure transducer (PT#2), allowing simultaneous determination of IOP, TM/SC IW interface pressure, and EVP in the model in a way that is not possible *in vivo*. The pressure differential between IOP and TM/SC IW tissue interface increased with IOP and outflow rate, reflecting different resistance in the TM compared with SC IW tissue as shown in Figures 8A-C.

Inherent to our modeling of TM with a needle resistor and SC IW with a one-way valve are the following major assumptions: (a) the TM is the outflow tract's site of major fluid drainage resistance and thus the major determinant of IOP; and that (b) while SC IW has intrinsic resistance, its key role is to sustain a pressure differential between the anterior chamber and SC. Our empiric data confirms the importance of TM resistance in establishing steady-state IOP above EVP. Under a constant pressure perfusion (feedback-controlled) setting in this model and in the absence of a needle resistor but presence of a one-way valve, unrestricted flow occurred when we sought to sustain IOP at a level above EVP (as seen in Figure 6). Unrestrained

outflow due to insufficient resistance makes it hard for IOP to approximate EVP let alone rise above it even if a one-way valve was present. Thus both the presence of the TM outflow resistance and a SC IW valve are necessary for IOP to be sustained above EVP. Below EVP, only the valve is necessary to maintain a differential between IOP and EVP. Here, SCIW (a) provides modest outflow resistance compared with the TM, (b) prevents retrograde flow into the anterior chamber (as seen in Figure 9B), and (c) allows for a pressure differential to exist between the anterior chamber and SC chamber, and thus for a pressure head to develop in the anterior chamber in a physiologic scenario with constant aqueous inflow.

Variants of pump flow control provided options to model aqueous humor dynamics under different scenarios. (1) Under constant pressure perfusion, the pump flow rate was made to represent outflow for a given steady state IOP, during which inflow into the conventional outflow tract equates trabecular outflow. Here, pump flow rate was automatically modulated by an electronic feedback loop between PT and pump to sustain a preset pressure (in PT#1, representing IOP). Constant pressure was predetermined with an analogue voltage controller as previously described.[68] (2) Under an alternative scenario of constant flow perfusion, the pump flow rate was made to represent a given fixed rate of aqueous production at a point in time. This allowed for equilibration of the aqueous dynamic to be observed under predetermined physiological conditions.

Chapter 4: Understanding abnormal outflow resistance and episcleral venous pressure in an artificial hydraulic model of the conventional aqueous drainage

The work associated with results and discussion of Chapter 4 was presented at the Association for Research in Vision and Ophthalmology Annual Meeting 2014 at Orlando, USA[71] and currently being prepared for submission as a paper for a journal article.

4.1 Results

4.1.1 Needle resistors simulate physiologic and pathologic conventional drainage resistance

Linear regression models for normal and high resistance needles were y=0.58x-0.05 (R^2=1.00; Figure 11A) and y=1.36x-0.06 (R^2=1.00; Figure 11B), respectively. Outflow resistance (slope) was approximately 2.3x greater in the high (1.36mmHg/µl/min) than normal resistance needle (0.58 mmHg/µl/min). Thus, modification of a needle resistor representing trabecular resistance in the model resulted in a needle with measurably increased resistance representing pathologically elevated trabecular resistance.

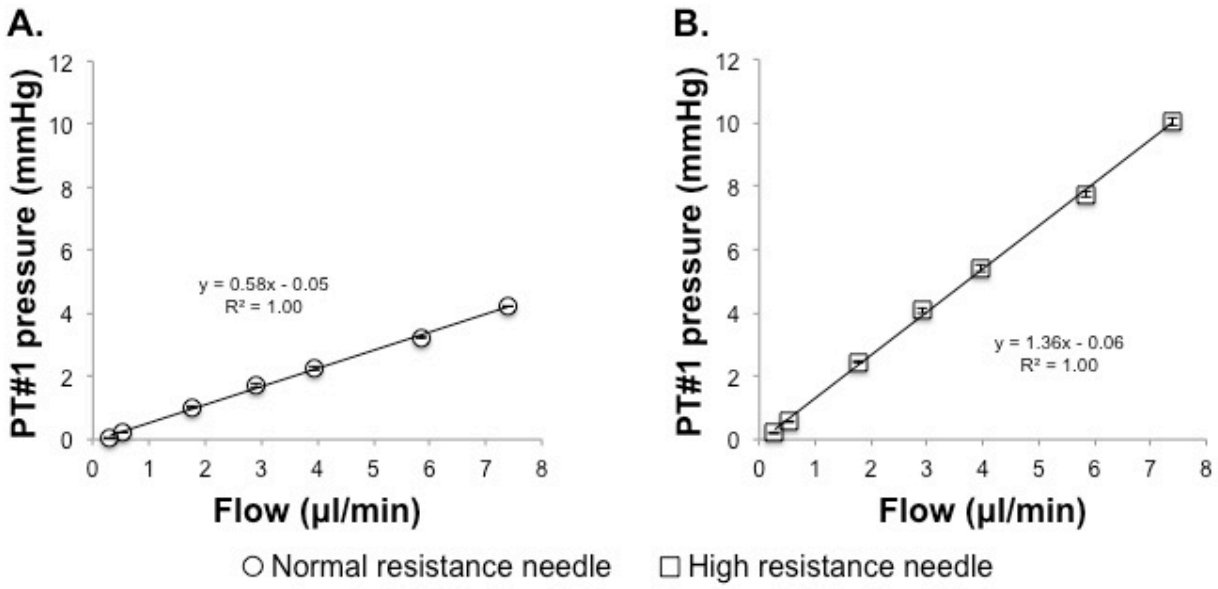

Figure 11. A. Relationship between pressure (PT#1) and flow rate in normal resistance needle using linear regression model (y=0.58x-0.05; R^2=1.00). **B.** Outflow resistance from high resistance needle using linear regression model (y=1.36x-0.06; R^2=1.00). Data plots and error bars (SEM) were based on triplicate measurements.

4.1.2 Higher trabecular resistance affects outflow relative to EVP

Under constant pressure perfusion, outflow was absent as long as PT#1 pressure (IOP) was below PT#3 (EVP) for both normal resistance needle (representing normal trabecular resistance; seen in a-e of Figure 12A) and high resistance needle (representing high trabecular resistance; seen in a'-e' of Figure 12B). Outflow commenced when PT#1 pressure exceeded PT#3. Flow rate were different; however, at commencement of outflow with similar PT#1 pressure (IOP) for both needles and just above PT#3 (EVP), flow through the normal resistance needle was 0.2µl/min (Figure 12A and 12C) and flow through the high resistance needle was 0.1µl/mi (Figure 12B and 12C). As pressure in PT#1 was increased above PT#3 (11mmHg) in 1mmHg increments, flow rate rose in both needles but at different rates. For equivalent PT#1 pressures (IOP) above PT#3 (EVP), flow rate (outflow) was higher in the normal resistance needle (seen in f-j of Figure 12A and 12C) than

in the high resistance needle (seen in f'-j' of Figure 12B and 12C). For example, when PT#1 was set at 15.3mmHg, flow rate in the normal resistance needle was 6.1µl/min and the flow rate in the high resistance needle was 2.4µl/min. Thus, the higher PT#1 was above PT#3, the greater the deviation in absolute flow rate seen between the normal and high resistance needles. For PT#1>PT#3, the relationship between pump flow rate (outflow) and PT#1 pressure (IOP) was linear (R^2=0.98-0.99), as shown in Figure 12D. Linear regression models indicated a higher hydraulic conductivity (2.7x; i.e., outflow facility) in the normal (y=1.50x-17.12) compared with the high (y=0.55x-6.18) resistance needle (also shown in Figure 12D). Thus, pathologically higher trabecular resistance is associated with a reduced rate of aqueous outflow compared with physiologic trabecular resistance at a given constant steady-state IOP above EVP.

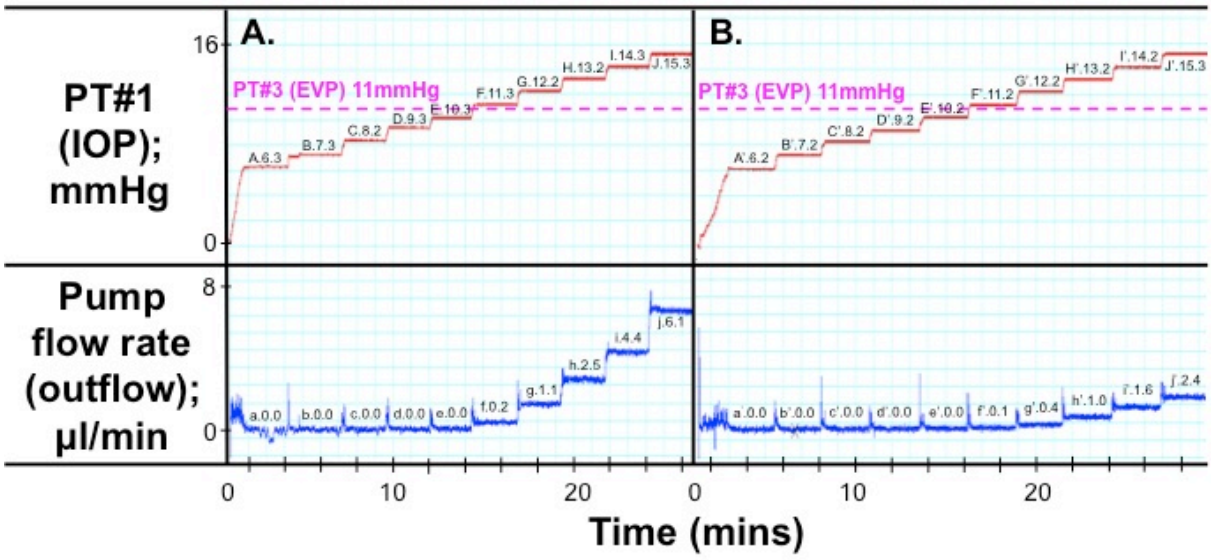

Figure 12. Representative tracings of PT#1 pressure (IOP; red) and pump flow rate (outflow; blue) with respect to PT#3 (EVP; pink) in a **(A)** normal resistance needle (representing normal trabecular resistance) and **(B)** high resistance needle (representing high trabecular resistance).

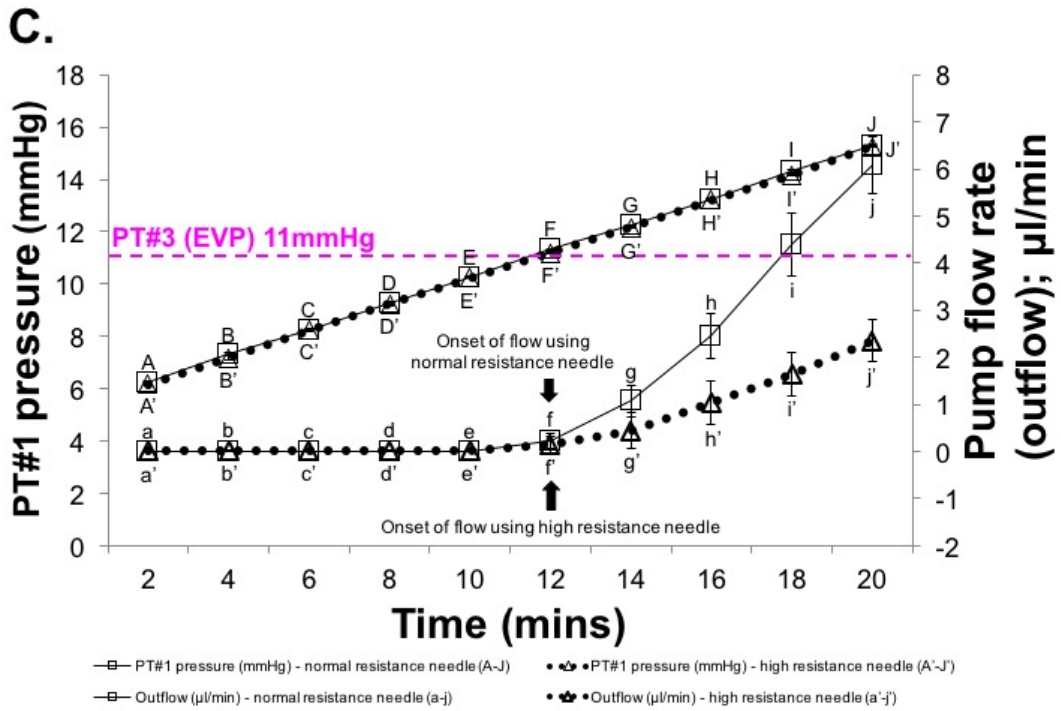

Figure 12C. Data plot for normal resistance needle (representing normal trabecular resistance) and high resistance needle (representing high trabecular resistance) of PT#1 pressure (IOP) and flow rate (outflow) with respect to PT#3 (EVP) over the time-course of an experiment based on triplicate measurements. Markers A-J and a-j correspond to similar markers in tracings of Figure 12A while markers A'-J' and a'-j' correspond to similar markers in tracings of Figure 12B. Data plots and error bars (SEM) were based on triplicate measurements.

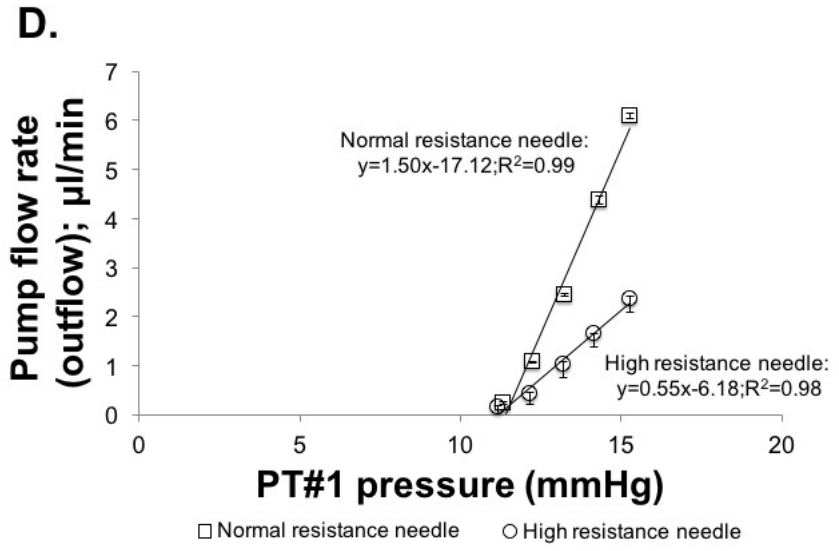

Figure 12D. Data plots showing the relationship between pump flow rate (outflow) and PT#1 pressure (IOP) for a normal resistance needle (square) and high resistance needle (circle). Plots were linear (R^2=0.98-0.99) with regression slopes representing outflow facility, which was 2.7x higher for normal resistance needle (y=1.50x-17.12) compared with high resistance needle (y=0.55x-6.18). Data plots and error bars (SEM) were based on triplicate measurements.

4.1.3 Increased trabecular resistance raises IOP under constant inflow

Constant flow perfusion mimics a condition of constant aqueous inflow, during which PT#1 pressure (IOP) is expected to vary with resistance as shown in Figures 13A-E. For a given constant flow rate, PT#1 pressure was greater in the high resistance needle (see A'-G' in Figure 13B) compared with normal resistance needle (see A-G in Figure 13A). The PT#1 pressure differential between normal and high resistance needle increased with perfusion flow rate. At a flow rate of 0.5µl/min, the pressure differential was 1.7mmHg but for a flow rate of 7.4µl/min, the pressure differential was 24.1mmHg. This corresponded with outflow resistance being 6x less in the normal ($y=0.65x+10.85$; $R^2=0.99$) compared with the high resistance ($y=3.90+11.05$; $R^2=1.00$) needle, as shown in Figure 13E. Thus, for a given aqueous flow rate, higher trabecular resistance is associated with higher IOP and also rising disproportionately with higher flow rates compared with normal trabecular resistance.

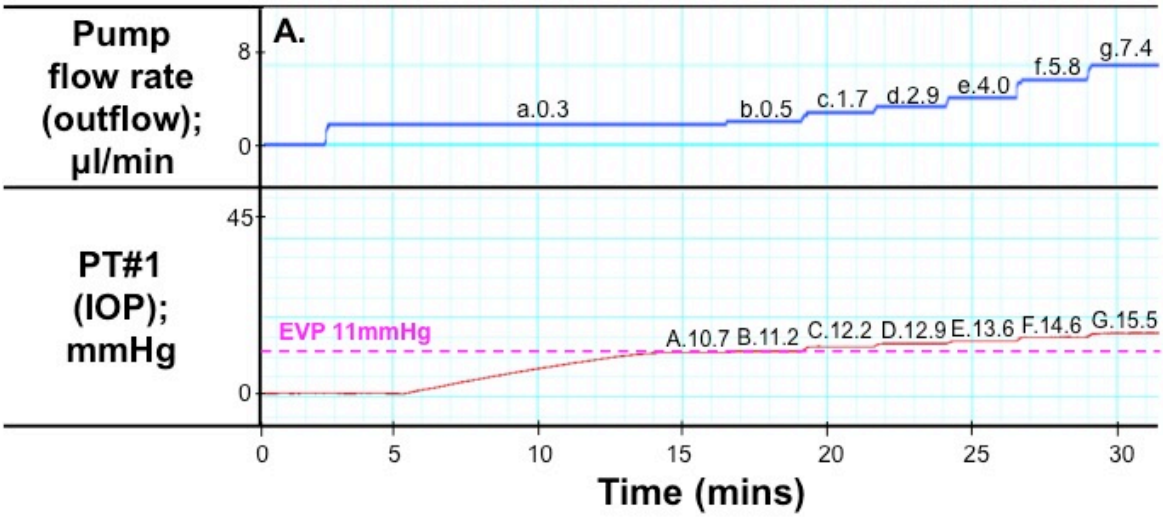

Figure 13A. Representative tracings showing how PT#1 pressure (IOP) varies with pump flow rate (inflow for IOP below EVP; outflow for IOP above EVP) in a normal resistance needle.

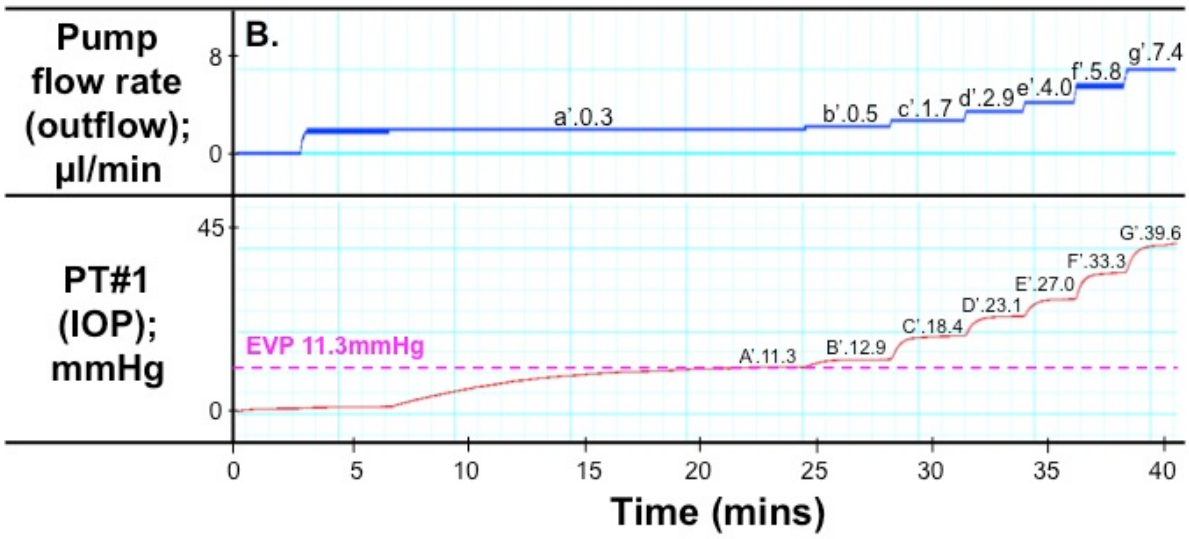

Figure 13B. Representative tracings showing how PT#1 pressure (IOP) varies with pump flow rate (inflow for IOP below EVP; outflow for IOP above EVP) in a high resistance needle.

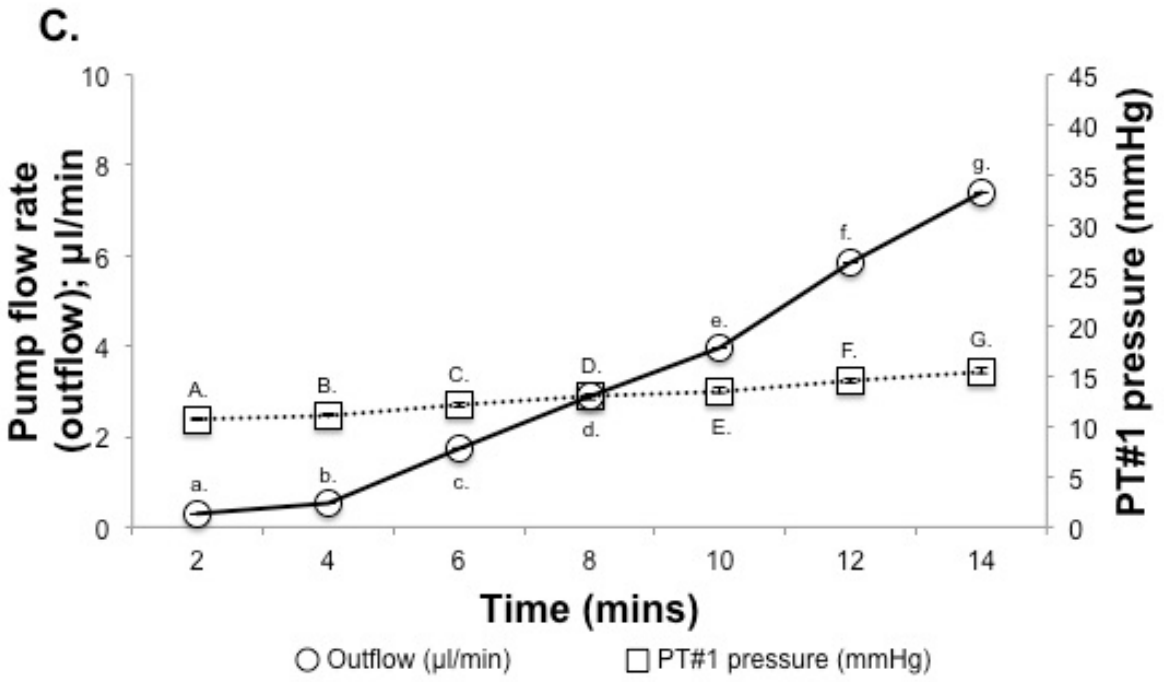

Figure 13C. Data plots showing relationship between constant pump flow rate (inflow for IOP below EVP; outflow for IOP above EVP) and PT#1 pressure (IOP) over the time-course of an experiment for a normal resistance needle and corresponded to the tracings in Figure 13A. Data plots and error bars (SEM) were based on triplicate measurements.

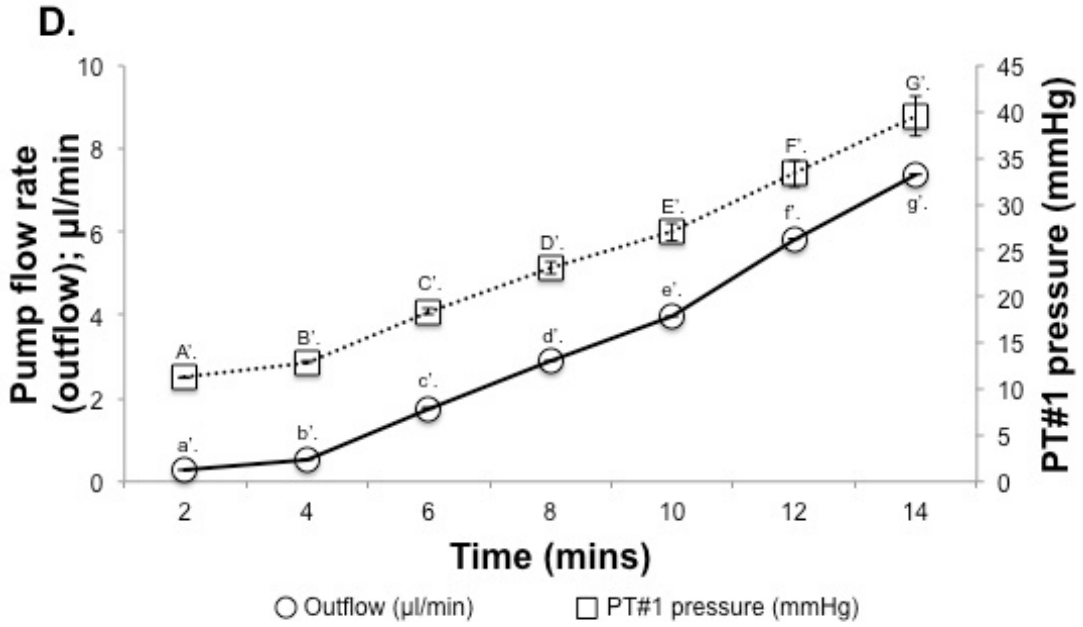

Figure 13D. Data plots showing relationship between constant pump flow rate (inflow for IOP below EVP; outflow for IOP above EVP) and PT#1 pressure (IOP) over the time-course of an experiment for a high resistance needle and corresponded to the tracings in Figure 13B. Data plots and error bars (SEM) were based on triplicate measurements.

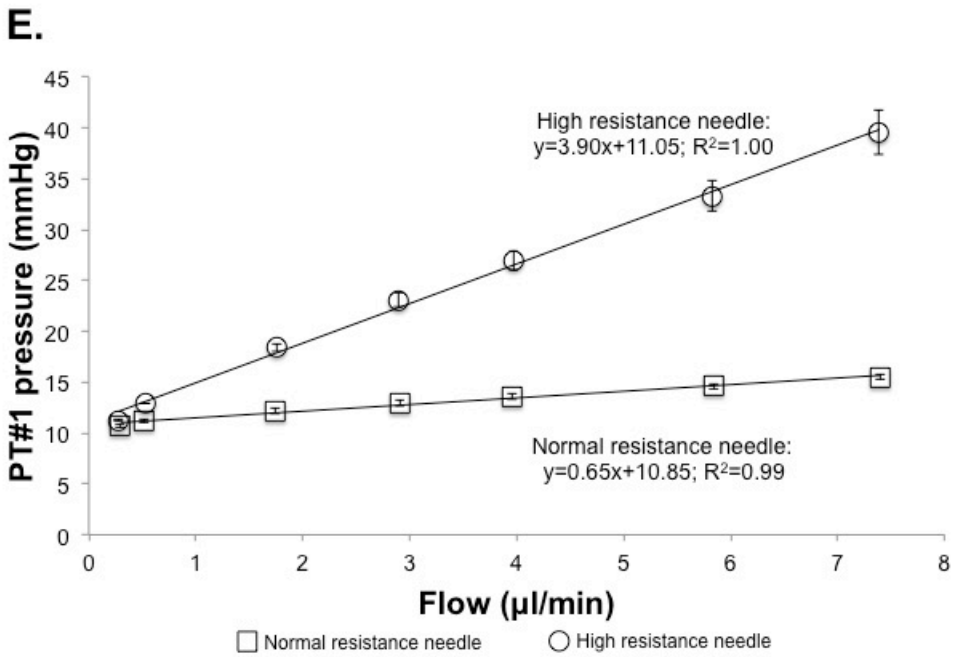

Figure 13E. Data plots showing a linear relationship (R^2=0.99-1.00) between PT#1 pressure (IOP) and constant pump flow rate for the normal (squares) and high (circles) resistance needles wherein slope of the regression function represents resistance of the respective needles (normal resistance needle: y=0.65x+10.85 versus high resistance needle: y=3.90x+11.05). For a given flow rate, PT#1 pressure (IOP) is higher with high resistance needle (high trabecular resistance). Data plots and error bars (SEM) were based on triplicate measurements.

4.1.4 IOP must rise to higher EVP for outflow to start

When EVP was raised from 11mmHg to 15mmHg, there was no outflow while PT#1 pressure (IOP) remained less than EVP under constant pressure perfusion. Onset of outflow commenced and continued to increase when PT#1 pressure levels (IOP) exceeded EVP. With EVP set at 11mmHg, outflow started when PT#1 was raised to 11.3mmHg (F in Figure 14A and 14C) but not when PT#1<EVP. Likewise when EVP was 15mmHg, PT#1 pressure (IOP) did not yield any outflow until it exceeded 15mmHg (G' in Figure 14B and 14D). Onset of outflow occurred later for EVP=15mmHg than EVP=11mmHg, as it took longer for PT#1 to rise above 15mmHg using a step-wise protocol of incrementally increasing constant pressure perfusion. Thus, outflow was responsive to the level of EVP. With higher EVP, IOP must rise accordingly to exceed EVP for outflow to occur.

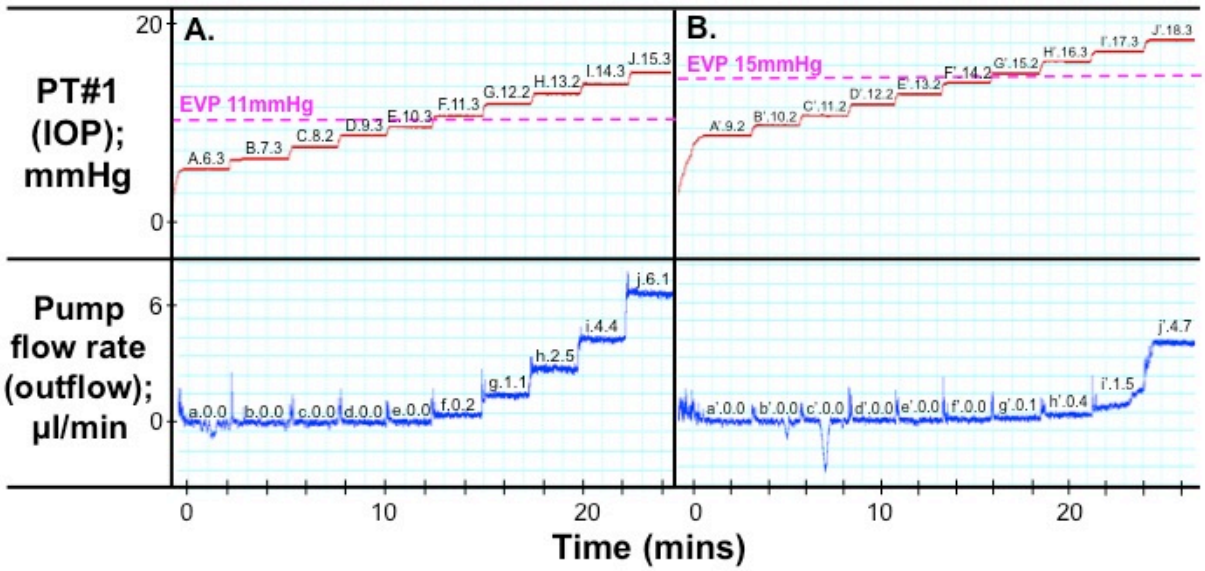

Figure 14. Representative tracings showing relationship between PT#1 (IOP) and pump flow rate (outflow) with EVP of 11mmHg **(A)** and 15mmHg **(B)**.

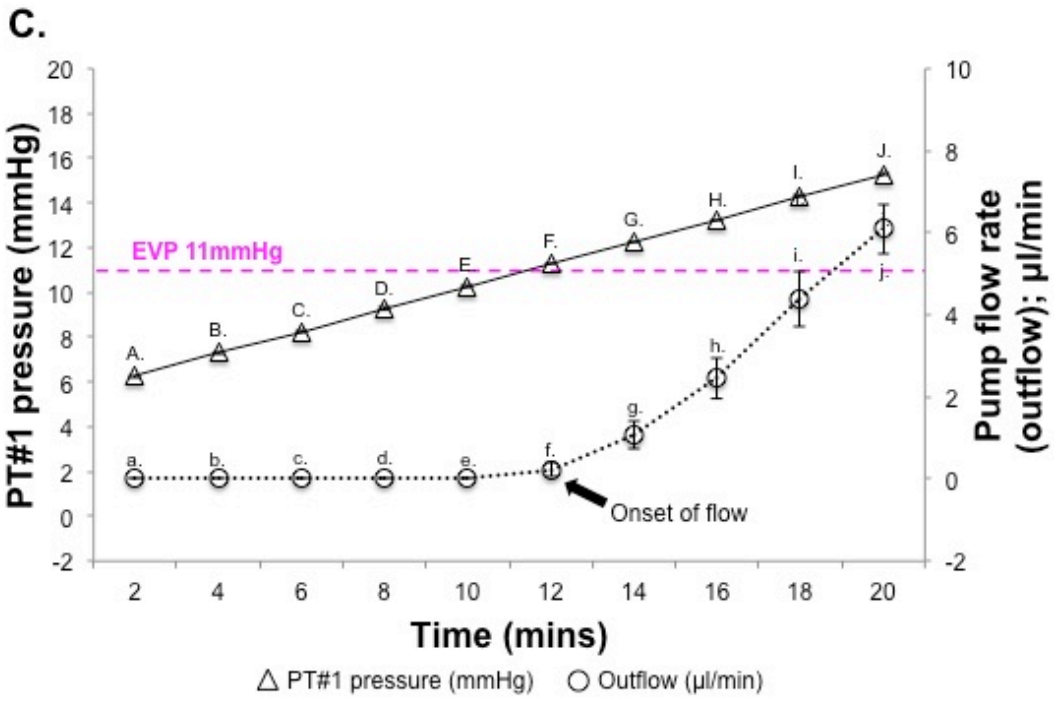

Figure 14C. Data plots showing relationship between PT#1 (IOP) and pump flow rate (outflow) over the time-course of an experiment relative to EVP=11mmHg and corresponded to the tracings in Figure 14A. Onset of flow occurred when PT#1 reached and exceeded EVP (see F and f). Data plots and error bars (SEM) were based on triplicate measurements.

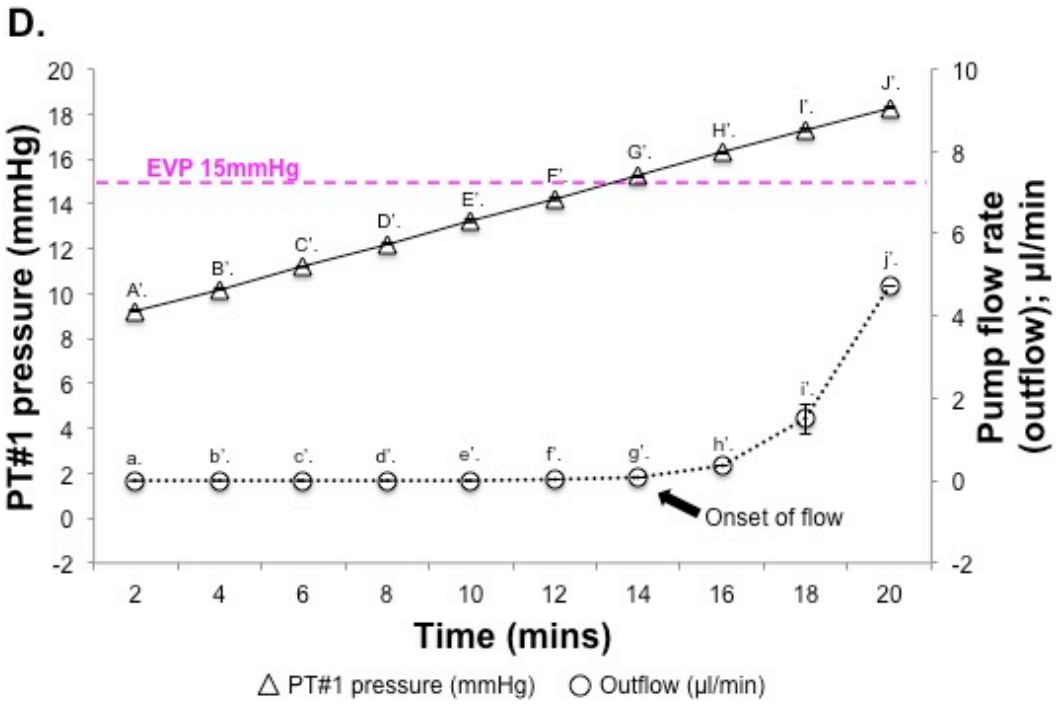

Figure 14D. Data plots showing relationship between PT#1 (IOP) and pump flow rate (outflow) over the time-course of an experiment relative to EVP=15mmHg and corresponded to the tracings in Figure 14B. Onset of flow occurred when PT#1 reached and exceeded PT#3 (see G' and g'). Data plots and error bars (SEM) were based on triplicate measurements.

4.1.5 IOP varies with EVP under constant inflow

For a given rate under constant flow perfusion (inflow rate), a higher PT#3 (EVP) pressure was associated with higher PT#1 (IOP), as shown in Figures 15A-D. As flow rate was gradually increased, PT#1 (IOP) pressure rose higher when EVP was 15mmHg (Figure 15B and 15D) compared when EVP was 11mmHg (Figure 15A and 15C). Linear regression models for the relationship between pressure (PT#1) and flow rate showed almost similar outflow resistances between EVP 11mmHg ($y=0.65x+10.85$; $R^2=0.99$) and 15mmHg ($y=0.59x+15.52$; $R^2=0.95$), as shown in Figure 15E. Higher EVP caused the pressure (PT#1; IOP) versus flow curve to be shifted upward so that for a given flow rate, PT#1 pressure (IOP) was always greater in the higher EVP in a way that was independent of outflow resistance. Thus, for a given aqueous inflow rate, IOP rises with EVP is due to an upward shift in the pressure-flow relationship rather than because of change in outflow resistance.

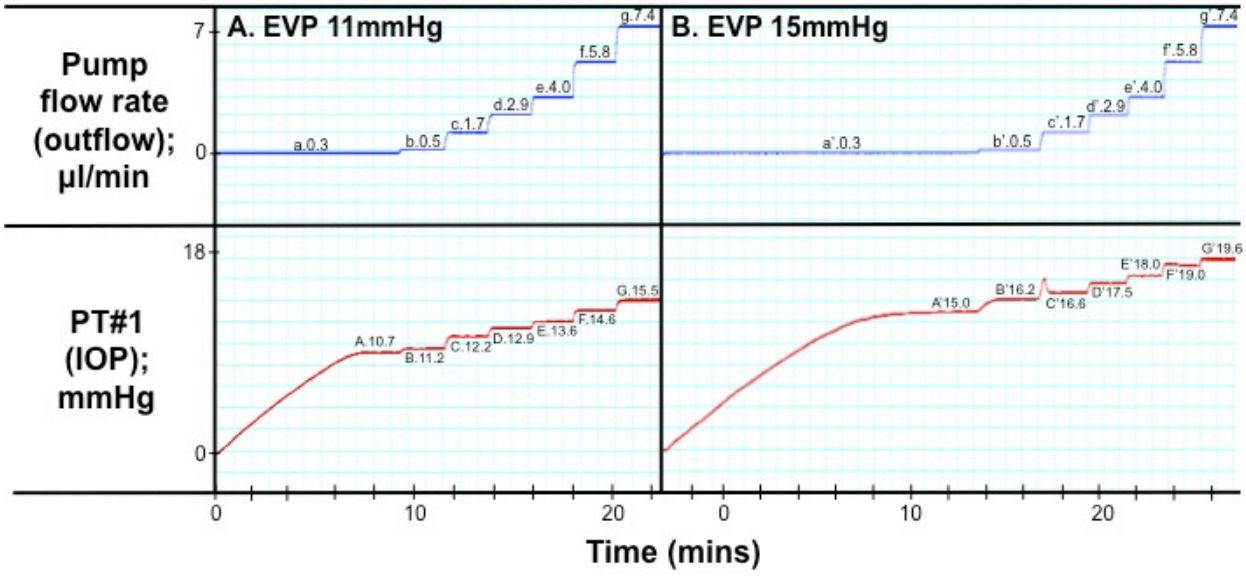

Figure 15. Representative tracings showing the relationship between pump flow rate (outflow) and PT#1 pressure (IOP) at two different PT#3 (EVP) pressures: **(A)** 11mmHg and; **(B)** 15mmHg under constant flow perfusion.

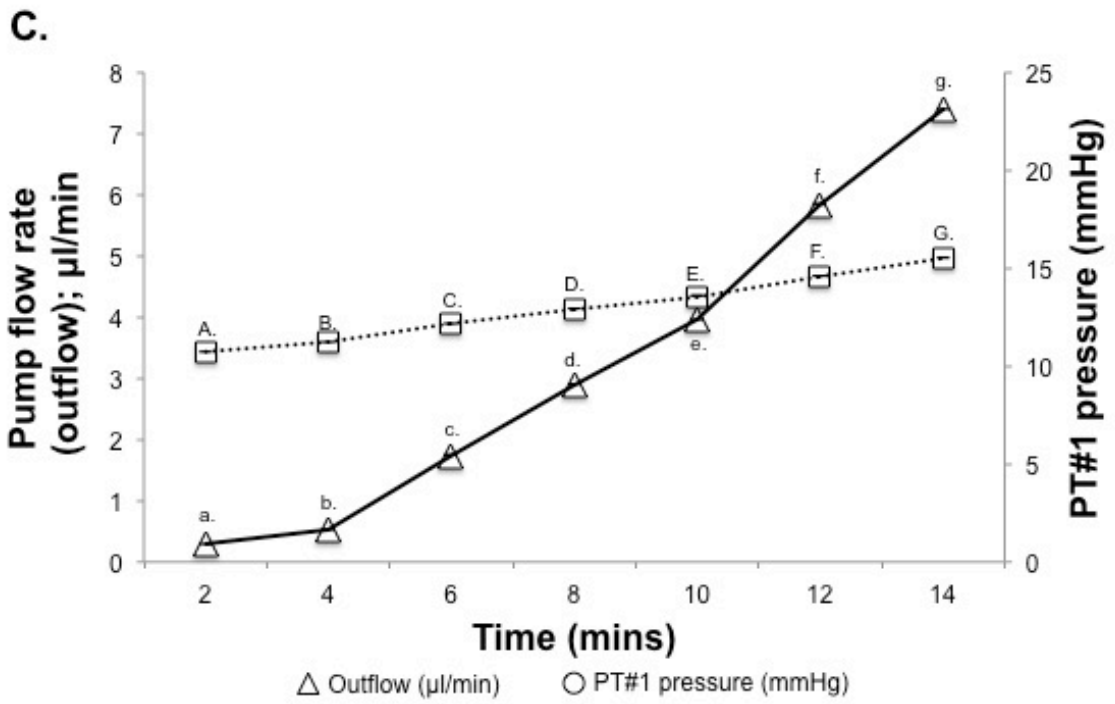

Figure 15C. Data plots showing the relationship between pump flow rate (outflow) and PT#1 pressure (IOP) with EVP=11mmHg over the time-course of a constant flow perfusion experiment and corresponded to tracings in Figure 15A. Data plots and error bars (SEM) were based on triplicate measurements.

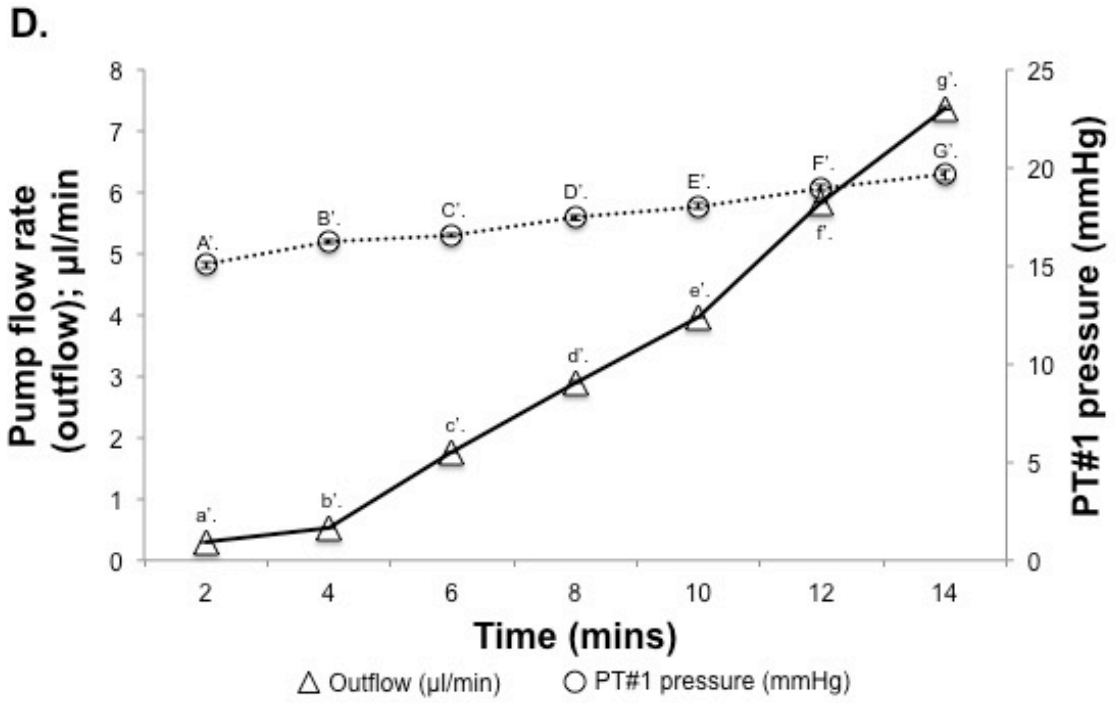

Figure 15D. Data plots showing the relationship between pump flow rate (outflow) and PT#1 pressure (IOP) with EVP=15mmHg over the time-course of a constant flow perfusion experiment and corresponded to tracings in Figure 15B. Data plots and error bars (SEM) were based on triplicate measurements.

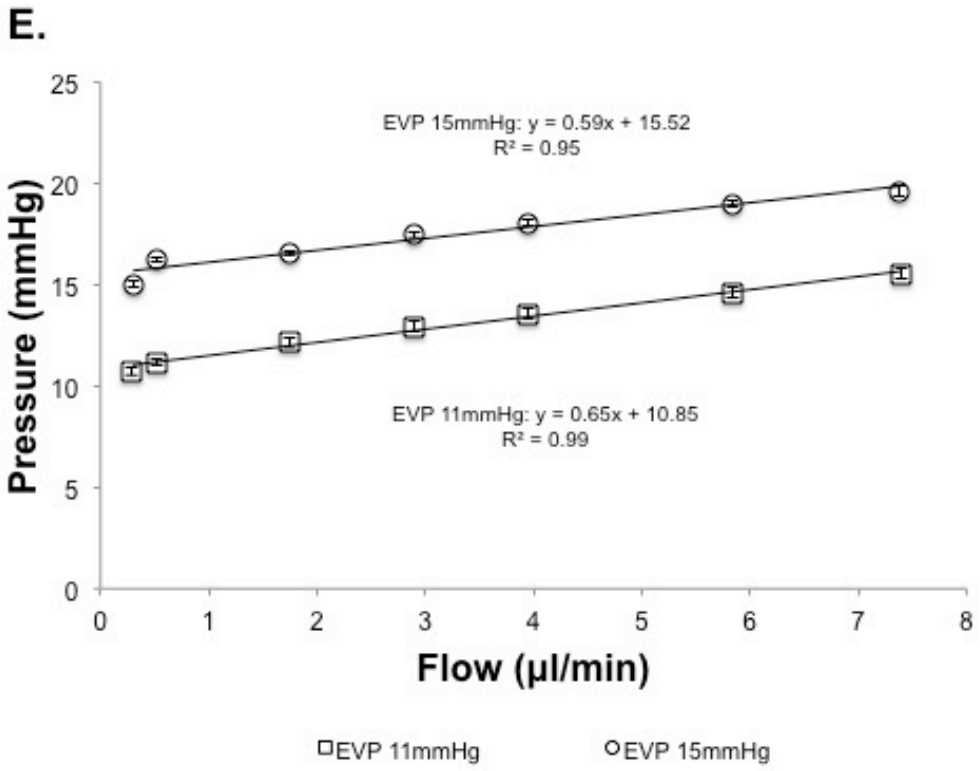

Figure 15E. Graphs showing linear relationship between pressure (PT#1; IOP) and flow rate for EVP levels of 11mmHg (y=0.65x+10.85; R^2=0.99) and 15mmHg (y=0.59x+15.52; R^2=0.95). The curve is shifted upward with higher EVP with slope (outflow resistance) relatively maintained.

4.1.6 Summary of results from simulation of the conventional outflow pathway under pathological conditions (elevated TM resistance and elevated EVP)

Essential aspects demonstrated from this simulation are listed below:

- The high resistance needle simulated pathologic TM resistance while the normal resistance needle simulated physiologic TM resistance.

- The degree of needle resistance affected the outflow rate and outflow facility. Under constant pressure perfusion, outflow rate and facility were lower with high resistance compared to normal resistance needle.

- The degree of needle resistance also influenced the level of IOP with greater IOP observed in high resistance compared to normal resistance needle under constant flow rate.

- In addition to needle resistance, the level of EVP affected the onset of outflow. Under constant pressure perfusion, higher EVP resulted to later onset of outflow as IOP needed to reach a higher EVP.

- Intraocular pressure was directly influenced by the level of EVP by an upward shift in the pressure-flow curve independent of outflow resistance. In this experiment, greater EVP resulted in higher IOP.

4.2 Discussion

By modifying certain components of the artificial perfusion system that simulated conventional outflow pathway under physiological conditions, this artificial hydraulic system was able to simulate two pathological scenarios of the said pathway mimicking: (1) glaucoma with elevated TM resistance by reducing the diameter of the 35G needle; and (2) secondary glaucoma from elevated EVP attained by increasing the fluid height of the distal fluid column. Results obtained from these modified components were compared to the experiments that simulated conventional outflow pathway under physiological conditions. Our results demonstrated that needle resistance affected flow rate (outflow) and outflow facility under constant pressure perfusion. In high resistance needle, flow rate and outflow facility (Figure 12B-D) were both lower versus normal resistance needle (Figure 12A, 12C and 12D). Furthermore, at a given constant flow rate (under constant flow perfusion), needle

resistance influenced level of IOP, with IOP greater in high resistance needle (Figure 13B and 13D) compared to normal resistance needle (Figure 13A and 13C). For EVP experiments under constant pressure perfusion, later onset of outflow occurred with EVP 15mmHg (Figure 14B and 14D) compared to EVP 11mmHg (Figure 14A and 14C) as PT#1 pressure (IOP) must reached a higher level of EVP for outflow to occur. Lastly, PT#1 pressure (IOP) was directly influenced by the level of EVP under constant pump flow rate. IOP was higher when EVP was set at 15mmHg (as shown in Figure 15B and 15D) compared to 11mmHg (as shown in Figure 15A and 15C). Higher IOP occurred from elevated pressure in the episcleral venous plexus and not from outflow resistance.

As mentioned earlier, elevated IOP is the only modifiable risk factor for glaucoma. The JC region of the TM and the SC IW endothelia are responsible for the resistance of aqueous humor outflow in the conventional pathway.[12-19] These structures contributed approximately 75% to 90% of total resistance to aqueous outflow in human[12] and nonhuman primate eyes[15], respectively. This resistance that generates IOP must be high enough for flow to occur across the TM/SC IW interface.[20] Any abnormalities to this structure can elevate IOP, as seen in glaucoma with elevated TM resistance. As expected, at a given constant aqueous flow rate, there was 6x more resistance in the high (3.90mmHg/µl/min) compared to the normal resistance needle (0.65mmHg/µl/min) resulting in higher IOP from the needle with greater resistance (Figure 13E). Furthermore, IOP rose disproportionately with increasing aqueous flow rate in the high compared to normal TM resistor. For example, when flow rate was initially set at 0.5µl/min, IOP was 12.9mmHg versus 11.2mmHg in the high versus normal resistance needle, respectively (Figure 13A-D).

As flow rate was increased to 7.4µl/min, IOP from the high resistance needle was 39.6mmHg compared to 15.5mmHg from the needle with normal resistance (Figure 13A-D). The observation of higher pressure from the high resistance needle was consistent with Poiseuille's law, which is:

$$R = 8\eta L/\pi r^4$$

where R is resistance, η is viscosity, L is length and r is radius of the tube. As resistance is inversely proportional to the radius to the fourth power, greater resistance was generated from the high resistance needle due to its smaller radius. Although the exact location (either the TM or SC IW) where the resistance originates in the conventional outflow pathway is still not entirely understood, Holmberg had described pores along the SC IW endothelia.[72] More recently, several investigators have studied pore density and its relationship to normal and glaucomatous eyes.[73-75] Johnson *et al* reported a five-fold increase in pore density in normal eyes compared to eyes with glaucoma.[75] Surprisingly, the diameter of pores between normal and glaucomatous eyes were found to be similar.[75] If decrease pore density was a definite reason for elevation of IOP in glaucoma, the principle of parallel resistance could be applied. The latter states that total resistance (regardless of diameter) is less than the lowest resistance of any given tube (or pore for this matter). This means that having more pores can less likely lead to increase resistance in the area of interest. This concept is similar to the low resistance seen in a capillary bed. Individual capillary has high resistance given their small diameter but as a whole group, these vessels contribute a very small part to the total vascular resistance.

This modified artificial hydraulic model also demonstrated that flow rate (outflow) and outflow facility in high resistance needle (Figure 12B and 12C) were

both lower compared to normal resistance needle (Figure 12A and 12C), where outflow facility in the high and normal resistance needle were 0.55µl/min/mmHg and 1.50µl/min/mmHg, respectively (Figure 12D). These findings were interestingly similar to previous studies. Grant's experiment in glaucomatous eyes (where outflow resistance was considered abnormally high) revealed reduced outflow rate and facility that was not present in normal eyes.[76] Several investigators also noted lower outflow facility and greater flow resistance with rising IOP or perfusion pressure in glaucomatous versus normal eyes.[42,77-80] This occurrence could be explained anatomically by a histologic study done on human and monkey eyes fixed at various levels of IOP that was less, equal or greater to EVP, and revealed that TM gradually expands as the lumen of the SC concurrently appeared occluded as IOP reached at least 30mmHg above EVP.[81] In that study, the occlusion of the SC lumen follows the fluid dynamics of a modified high resistance needle observed in this study.

In addition to TM resistance, EVP contributes directly to IOP as represented by the classic Goldmann's equation, which is:

$$IOP = F/C_{trab} + P_e$$

wherein F is aqueous inflow into the trabecular pathway; C_{trab} is outflow facility through the trabecular route and P_e is EVP.[82] This perfusion system demonstrated that the level of EVP influenced onset of outflow under constant pressure perfusion. With EVP 15mmHg, onset of flow rate occurred later (Figure 14B and 14D) compared to 11mmHg (Figure 14A and 14C), as pressure in PT#1 (IOP) needed to buildup to meet a higher EVP. With constant pump flow rate, this model demonstrated that EVP (PT#3) can directly influenced IOP. By comparing two levels of EVP (11 and 15mmHg), IOP was higher with EVP 15mmHg compared to 11mHg,

findings consistent with the classic Goldmann's equation. At a given constant flow rate, the level of EVP will affect IOP (i.e. IOP will always be higher with elevated EVP). For example, at flow rate of 2.9μ/l (see d in Figure 15A and 15B), the corresponding IOP was 12.9mmHg at EVP 11mmHg (Figure 15A and 15C) while IOP was 17.5mmHg at EVP 15mmHg (Figure 15B and 15D). This relationship coincided with Friberg *et al*, which they estimated that for every 0.83+/- 0.21mmHg change in EVP, this corresponded to 1mmHg change in IOP.[83] Furthermore, elevated EVP (due to abnormal aqueous outflow) causing secondary glaucoma include the following conditions: arteriovenous anomalies (including cavernous sinus fistula), venous obstruction (including thyroid ophthalmopathy, retrobulbar tumor, superior vena cava obstruction) and Sturge-Weber syndrome.[84] Since aqueous outflow was affected from the above-mentioned disease process, IOP becomes elevated because aqueous outflow would need to reach the abnormally high pressures found in the episcleral venous plexuses which gets transmitted to the anterior chamber. Furthermore, outflow resistance was almost similar between these two levels of EVP (EVP 11mmHg: 0.65mmHg/μl/min versus EVP 15mmHg: 0.59mmHg/μl/min) as shown in Figure 15E. With these observations, this suggested that elevated EVP was from an upward shift in the pressure-flow relationship curve rather than change in outflow resistance. Our observation that EVP directly influenced IOP suggested that EVP in glaucomatous eyes would be higher than in normal healthy eyes, which has been demonstrated by previous studies. Linner and Leith reported EVP between 10.95+/- 0.274mmHg and 11.76+/-1.58mmHg in glaucomatous eyes and between 10.45+/-0.212 and 10.99+/-1.41mmHg in normal eyes.[85,86] Selbach *et al* also reported that EVP was higher in primary open angle glaucoma (12.1+/-0.5mmHg) and normal tension glaucoma (11.6mmHg+/-0.4mmHg) compared to controls (9.5+/-

0.2mmHg).[82] Conversely, other groups demonstrated EVP between 8mmHg-9.3mmHg in glaucomatous eyes[87-92] lower than their corresponding control groups. The different results could be explained on the basis that methodology to measure EVP was not identical.

Chapter 5. Limitations, conclusion and future directions

The following limitations were identified from this study. (1) Modification of the 35G needle was done by gently clamping the needle tip, however, the force required to alter the needle was not taken into account. It might be worthwhile to know the amount of force required to modify the needle diameter associated to a specific resistance. One solution would be to obtain a needle with a diameter smaller than the 35G needle and with Poiseuille's law, the radius of the needle could predict its corresponding resistance. Another option would be to use a number of small low volume syringe filters that can either be incorporated or removed to incrementally simulate increase or decrease outflow resistance, respectively. This approach however, may not work given the minute amount of volume used in this model (50µl per microsyringe) to represent aqueous inflow relative to the size of syringe filters. (2) This perfusion system was constructed from non-biological materials that limits in achieving an all-inclusive model to simulate aqueous humor dynamics. Recent work using multiple layers of human TM cells grown on a bioengineered scaffold revealed promising results.[44] However, their perfusion setup consisted of a scaffold containing only human TM cells and lacks various components of the conventional outflow pathway that were present in our setup. With our system, the one-way valve and the 35G needle could be potentially substituted with human TM and SC IW endothelial cells potentially creating a more robust model. (3) This system lacks components distal to the SC such as collector channels. In addition to the TM and SC IW endothelium, there is evidence to suggest that these channels also contribute to outflow resistance such as the presence of residual resistance of 25% post trabeculotomy in enucleated eye[12,93,94] and a recent study theorized that dilated collector channels could decrease IOP.[94,95] Furthermore, bypassing trabecular

resistance, which is one of the aims of MIGS,[96-98] could be recreated in this model by removing the TM needle resistor and SC IW one-way valve. If by implication the pressure differential between the simulated anterior chamber and SC chamber were to be removed, this will result in equalization of IOP and EVP (as similar to what was observed in Figure 9A) and outflow would not occur. However, this does not conform to current observation in MIGS.[96-98] This suggests that there is another area of resistance distal to the SC IW (i.e. collector channel resistance) and inclusion of the collector channels into the model is a part of a future study.

Findings from this artificial hydraulic system suggested that the conventional outflow dynamics under physiological conditions as well as pathological scenarios relating to outflow resistance and EVP were simulated. Main points observed while simulating the physiologic conventional outflow pathway in an artificial hydraulic model are summarize below.

1. Two separate outflow resistance (simulated TM from the 35G needle and simulated SC IW from the one-way valve) contributed to the total outflow resistance in this model. Outflow resistance in the needle resistor was higher than the valve.

2. Onset and cessation of outflow were determined by the relationship between IOP and EVP. Outflow commenced when PT#1 (IOP) reached and exceeded EVP (PT#3) and outflow ceased when EVP became higher than IOP.

3. The outflow resistor (35G needle) was essential in sustaining the IOP-EVP pressure gradient and pressure-dependent outflow as well as the establishment of a pressure gradient between the TM and SC IW (in the presence of outflow).

4. The one-way valve was responsible for the pressure differential between the simulated anterior chamber and SC. For example, without the valve, pressure equilibrated across all fluid compartments upon opening of the stopcock connected to the fluid column.

5. With constant aqueous inflow, IOP rose linearly as it reached the level of EVP. Once at this level, constant flow rate yields a constant IOP determined by outflow resistance.

In addition, major points observed from the pathologic conventional drainage in an artificial hydraulic model include the following:

1. Normal and high resistance needles simulated physiologic and pathologic trabecular resistance, respectively.

2. Outflow rate and outflow facility were affected by the nature of TM needle resistor (i.e., lower outflow rate and outflow facility were observed in the high resistance needle under constant pressure perfusion).

3. Level of IOP varied with needle resistance (i.e., higher IOP was observed with high resistance needle under a constant flow rate).

4. With elevated EVP, outflow occurred later as IOP has to reach a higher EVP under constant pressure perfusion.

5. Level of EVP directly influenced IOP (i.e., elevated EVP resulted in higher IOP) due to an upward shift in the pressure-flow curve independent of outflow resistance.

Future modification of other parameters of the hydraulic model to test alternative assumptions and hypotheses could be carried out. For example, a valve with higher resistance could be used to test the possibility that SC IW is a bigger determinant of physiological or pathological outflow resistance than what was modeled here. Further, analysis of the trans-TM and trans-SC pressure gradients in the setting of high TM resistance is a possibility as this model has the capacity to separate the TM resistor and SC IW valve. While rigid, non-compliant components was used, a modified setup may include substitution of current noncompliant tubing with compliant tubing for the SC chamber, necessary to simulate dynamic changes in this region. Instead of constant flow in the model, pump perfusion could be programmed to provide pulsatile flow. The distal column that provides constant EVP could itself be substituted with a pump that varies EVP in a cyclical manner to analyze the effect of venous pulsation on aqueous outflow dynamics. Further expansion of this present model includes incorporating a parallel non-pressure dependent (or minimally pressure dependent) uveoscleral outflow pathway. This

would allow us to simulate the complete aqueous outflow dynamic, including the potential to determine the relationship between aqueous humor dynamics and aging, which is otherwise hard to perform *in vivo* or *ex vivo*. Outflow rate through the uveoscleral tract was noted to be lower in aging compared to younger human[9-11,99] and primate[99] eyes. With an uveoscleral arm, there is a potential for this model to allow future studies to involve aging and pathological scenarios such as simulating higher outflow resistance in the non-conventional outflow pathway. Other options include to replicate collector channel resistance by incorporating another pressure transducer (called PT#4; to measure simulated collector channel pressure) distal to the SC chamber and connected serially to another 35G needle (simulating collector channels) as well as; to substitute or supplement the needle resistor with cultured TM cells on a suitable substrate to study TM cellular roles in outflow resistance. Similarly, the one-way valve may be replaced by cultured SC endothelial cells to test their putative valve-like behavior and resistance. A more elaborate model incorporating TM and SC cellular systems in series is a further option. These suggestions will be the subject of future studies to further model and characterize the aqueous outflow tract in health and glaucoma.

References

1. Quigley HA, Broman AT. The number of people with glaucoma worldwide in 2010 and 2020. Br J Ophthalmol. 2006;90:262-267.

2. Cook C, Foster P. Epidemiology of glaucoma: what's new? Can J Ophthalmol. 2012;47:223-226.

3. Weinreb RN, Aung T, Medeiros FA. The pathophysiology and treatement of glaucoma – a review. JAMA. 2014;311:1901-1911.

4. Resnikofff S, Pascolini D, Etya'ale D, et al. Global data on visual impairment in the year 2002. Bull World Health Organ. 2004;82:844-845.

5. Quigley HA. Glaucoma. Lancet. 2011;377:1367-1377.

6. King A, Azuara-Blanco A, Tuulonen A. Glaucoma. BMJ. 2013;346:1-9.

7. Bill A. Editorial: The drainage of aqueous humor. Invest Ophthalmol. 1975;14:1-3.

8. Toris CB. Pharmacotherapies for glaucoma. Curr Mol Med. 2010;10:824-840.

9. Toris CB, Yablonski ME, Wang YL, Camras CB. Aqueous Humor Dynamics in the Aging Human Eye. Am J Ophthalmol. 1999;127:407-412.

10. Toris CB, Koepsell SA, Yablonski ME, Camras CB. Aqueous humor dynamics in ocular hypertensive patients. J Glaucoma. 2002;11:253-258.

11. Johnson TV, Fan S, Camras CB, Toris CB. Aqueous humor dynamics in exfoliation syndrome. Arch Ophthalmol. 2008;126:914-920.

12. Grant WM. Further studies on facility of flow through the trabecular meshwork. Arch Ophthalmol. 1958;60:523-533.

13. Grant WM. Experimental aqueous perfusion in enucleated human eyes. Arch Ophthalmol. 1963;69:783-801.

14. Seiler T, Wollensak J. The resistance of the trabecular meshwork to aqueous humor outflow. Graefes Arch Clin Exp Ophthalmol. 1985;223:88-91.

15. Maepea O, Bill A. The pressures in the episcleral veins, Schlemm's canal and the trabecular meshwork in monkeys: effects of changes in intraocular pressure. Exp. Eye Res. 1989;49:645-663.

16. Maepea O, Bill A. Pressures in the juxtacanalicular tissue and Schlemm's canal in monkeys. Exp. Eye Res. 1992;54:879-883.

17. Ethier CR, Coloma FM, de Kater AW, et al. Retroperfusion studies of the aqueous outflow system. Part 2: Studies in human eyes. Invest. Ophthalmol. Vis. Sci. 1995;36:2466-2475.

18. Johnson M. What controls aqueous humour outflow resistance?. Exp Eye Res. 2006;82:545-557.

19. Overby DR, Stamer WD, Johnson M. The changing paradigm of outflow resistance generation: Towards synergistic models of the JCT and inner wall endothelium. Exp Eye Res. 2009;88:656-670.

20. Tamm ER. The trabecular meshwork outflow pathways: structural and functional aspects. Exp Eye Res. 2009;88:648-655.

21. Goldmann H. Abflussdruck, minutenvolumen und Widerstand der Kammerwasser Stromung des Menschen. Doc. Ophthalmol. 1951;5:278–356.

22. Malihi M, Sit AJ. Aqueous humor dynamics and implications for clinical practice. Int Ophthalmol Clin. 2011;51:119-139.

23. Braunger BM, Fuchshofer R, Tamm ER. The aqueous humor outflow pathways in glaucoma: A unifying concept of disease mechanisms and causative treatment. Eur J Pharm Biopharm. 2015;95:173-181.

24. Maier PC, Funk J, Schwarzer G, et al. Treatment of ocular hypertension and open angle glaucoma: meta-analysis of randomised controlled trials. BMJ. 2005;331:1-6.

25. Boland MV, Ervin AM, Friedman DS, et al. Comparative effectiveness of treatments for open-angle glaucoma: a systematic review for the US Preventive Services Task Force. Ann Intern Med. 2013;158:271-279.

26. Sit AJ. Optimizing conventional trabecular meshwork outflow. Methods by which to module flow though this pathway. Glaucoma Today. 2013;Sept/Oct: 39-42.

27. Garnock-Jones KP. Ripasudil: first global approval. Drugs. 2014;74:2211-2215.

28. Wang SK, Chang RT. An emerging treatment option for glaucoma: Rho kinase inhibitors. Clin Ophthalmol. 2014;9:883-890.

29. Polansky JR, Weinreb RN, Baxter JD, et al. Human trabecular cells. I. Establishment in tissue culture and growth characteristics. Invest Ophthalmol Vis Sci. 1979;18:1043-1049.

30. Alvarado JA, Wood I, Polansky JR. Human trabecular cells. II. Growth pattern and ultrastructural characteristics. Invest Ophthalmol Vis Sci. 1982;23:464-478.

31. Tripathi RC, Tripathi BJ. Human trabecular endothelium, corneal endothelium, keratocytes, and scleral fibroblasts in primary cell culture. A comparative study

of growth characteristics, morphology, and phagocytic activity by light and scanning electron microscopy. Exp Eye Res. 1982;35:611-624.

32. Weinreb RN, Mitchell MD, Polansky JR. Prostaglandin production by human trabecular cells: in vitro inhibition by dexamethasone. Invest Ophthalmol Vis Sci. 1983;24:1541-1545.

33. Polansky JR, Wood IS, Maglio MT, et al. Trabecular meshwork cell culture in glaucoma research: evaluation of biological activity and structural properties of human trabecular cells in vitro. Ophthalmology. 1984;91:580-595.

34. Polansky JR, Fauss DJ, Chen P, et al. Cellular pharmacology and molecular biology of the trabecular meshwork inducible glucocorticoid response gene product. Ophthalmologica. 1997;211:126-139.

35. Tamm ER, Russell P, Epstein DL, et al. Modulation of myocilin/TIGR expression in human trabecular meshwork. Invest Ophthalmol Vis Sci. 1999;40:2577-2582.

36. Tumminia SJ, Mitton KP, Arora J, et al. Mechanical stretch alters the actin cytoskeletal network and signal transduction in human trabecular meshwork cells. Invest Ophthalmol Vis Sci. 1998;39:1361-1371.

37. Vittal V, Rose A, Gregory KE, et al. Changes in gene expression by trabecular meshwork cells in response to mechanical stretching. Invest. Ophthalmol. Vis.

Sci. 2005;46:2857–2868.

38. Johnson DH, Tschumper RC. Human trabecular meshwork organ culture. A new method. Invest Ophthalmol Vis Sci. 1987;28:945-953.

39. Weinreb RN, Lindsey JD. The importance of models in glaucoma research. J Glaucoma. 2005;14:302-304.

40. Acott TS, Kingsley PD, Samples JR, et al. Human trabecular meshwork organ culture: morphology and glycosaminoglycan synthesis. Invest Ophthalmol Vis Sci. 1988;29:90-100.

41. Erickson LK, Rohen JW, Grant WM. Outflow facility studies in the perfused bovine aqueous outflow pathways. Curr Eye Res. 1988;8:799-807.

42. Erickson LK, Rohen JW, Grant WM, Outflow facility studies in the perfused human ocular anterior segment. Exp Eye Res. 1991;52:723-731.

43. Perkins TW, Alvarado JA, Polansky JR, et al. Trabecular meshwork cells grown on filters. Conductivity and cytochalasin effects. Invest Ophthalmol Vis Sci. 1988;29:1836-1846

44. Torrejon KY, Pu D, Bergkvist M, et al. Recreating a human trabecular meshwork outflow system on microfabricated porous structures. Biotechnol Bioeng. 2013;110:3205-3218.

45. Ethier CR, Kamm RD, Palaszewski BA, et al. Calculations of flow resistance in the juxtacanalicular meshwork. Invest Ophthalmol Vis Sci. 1986;27:1741-1750.

46. Villamarin A, Roy S, Hasballa R, Vardoulis O, Reymond P, Stergiopulos N. 3D simulation of the aqueous flow in the human eye. Med Eng Phys. 2012;34:1462-1470.

47. Peterson JA, Tian B, Bershadsky AD, et al. Latrunculin-A increases outflow facility in the monkey. Invest Ophthalmol Vis Sci. 1999;40:931-941.

48. Peterson JA, Tian B, Geiger B, et al. Effect of latrunculin-B on outflow facility in monkeys. Exp Eye Res. 2000:70:307-313.

49. Ko MK, Kim EK, Tan JCH. Glaucoma drug studies in live mice: effect of latrunculin-B on outflow facility and actomyosin contractility. Invest Ophthalmol Vis Sci. 2014;55:5674.

50. Barany EH. Simultaneous measurement of changing intraocular pressure and outflow facility in the vervet monkey by constant pressure infusion. Invest Ophthalmol Vis Sci. 1964;3:135-143.

51. Erickson KA, Kaufman PL. Comparative effects of three ocular perfusates on outflow facility in the cynomolgus monkey. Curr Eye Res. 1981;1:211-216.

52. Tian B, Kaufman PL. Effects of the Rho kinase inhibitor Y-27632 and the phosphatase inhibitor calyculin A on outflow facility in monkeys. Exp Eye Res. 2005;80:215-225.

53. Aihara M, Lindsey JD, Weinreb RN. Aqueous humor dynamics in mice. Invest Ophthalmol Vis Sci. 2003;44:5168-5173.

54. Millar JC, Clark AF, Pang IH. Assessment of aqueous humor dynamics in the mouse by a novel method of constant-flow infusion. Invest Ophthalmol Vis Sci. 2011;52:685-694.

55. Boussommier-Calleja A, Bertrand J, Woodward DF, et al. Pharmacologic manipulation of conventional outflow facility in ex vivo mouse eyes. Invest Ophthalmol Vis Sci. 2012;53:5838-5845.

56. John SW, Smith RS, Savinova OV. Essential iris atrophy, pigment dispersion and glaucoma in DBA/2J mice. Invest Ophthalmol Vis Sci. 1998;39:951-962.

57. Aihara M, Lindsey JD, Weinreb RN. Ocular hypertension in mice with a targeted type 1 collagen mutation. Invest Ophthalmol Vis Sci. 2003;44:1581-1585.

58. Senatorov V, Malyukova I, Fariss R, et al. Expression of mutated mouse myocilin induces open-angle glaucoma in transgenic mice. J Neurosci. 2006;26:11903-11914.

59. John SW, Hagaman JR, MacTaggart TE, et al. Intraocular pressure in inbred mouse strains. Invest Ophthalmol Vis Sci. 1997;38:249–253.

60. Danias J, Kontiola AI, Filippopoulos T, et al. Method for the noninvasive measurement of intraocular pressure in mice. Invest Ophthalmol Vis Sci. 2003;44:1138–1141.

61. Wang WH, Millar JC, Pang IH, et al. Noninvasive measurement of rodent intraocular pressure with a rebound tonometer. Invest Ophthalmol Vis Sci. 2005;46:4617–21.

62. Johnson TV, Fan S, Toris CB. Rebound tonometry in conscious, conditioned mice avoids the acute and profound effects of anesthesia on intraocular pressure. J Ocul Pharmacol Ther. 2008;24:175–185.

63. Ding C, Wang P, Tian N. Effect of general anesthetics on IOP in elevated IOP mouse model. Exp Eye Res. 2011;92:512–520.

64. Gaasterland DE Pederson JE, MacLellan HM. Perfusate effects upon resistance to aqueous humor ouflow in the rhesus monkey eye. A comparison

of glutathione-bicarbonate Ringer's solution to pooled aqueous humor as perfusate. Invest Ophthalmol Vis Sci. 1978;17:391-397.

65. Gaasterland DE, Pederson JE, MacLellan HM, et al. Rhesus monkey aqueous humor composition and a primate ocular perfusate. Invest Ophthalmol Vis Sci. 1979;18-1139-1150.

66. Erickson-Lamy K, Shroeder AM, Bassett-Chu S, et al. Absence of time-dependent facility increase ("washout") in the perfused enucleated human eyes. Invest Ophthalmol Vis Sci. 1990;31:2384-2388.

67. Scott PA, Overby DR, Freddo TF, et al. Comparative studies between species that do and do not exhibit the washout effect. Exp Eye Res. 2007;84:435-443.

68. Ko MK, Yelenskiy A, Gonzalez JM Jr, et al. Feedback-controlled constant-pressure anterior chamber perfusion in live mice. Mol Vis. 2014;20:163-170.

69. STH. Pump controller owner's guide. ADInstruments Pty Ltd, Bella Vista, Australia, 2005.

70. Kim EY, Chu E, Yelenskiy A, et al. Artificial simulation of conventional aqueous humor outflow dynamics. Invest Ophthalmol Vis Sci. 2013;54:3561.

71. Tan JCH, Chu ER, Gonzalez JM, et al. Simulating the effect of trabecular meshwork resistance and episcleral venous pressure on conventional

aqueous humor outflow dynamics. Invest Ophthalmol Vis Sci. 2014;55:2885.

72. Holmberg A. The fine structure of the inner wall of Schlemm's canal. Arch Ophthalmol. 1959;62:956-958.

73. Allingham RR, de Kater AW, Ethier CR, et al. The relationship between pore density and outflow facility in human eyes. Invest Ophthalmol Vis Sci. 1992;33:1661-1669.

74. Sit AJ, Coloma FM, Ethier CR, et al. Factors affecting the pores of the inner wall endothelium of Schlemm's canal. Invest Ophthalmol Vis Sci. 1997;38:1517-1525.

75. Johnson M, Chan D, Read AT, et al. The pore density in the inner wall endothelium of Schlemm's canal of glaucomatous eyes. Invest Ophthalmol Vis Sci. 2002;43:2950-2955.

76. Grant WM. Clinical measurements of aqueous outflow. Arch Ophthalmol. 1951;46:113-131.

77. Ellingsen BA, Grant WM. The relationship of pressure and aqueous outflow in enucleated human eyes. Invest Ophthalmol Vis Sci. 1971;10:430-437.

78. Brubaker RF. The effect of intraocular pressure on conventional outflow resistance in the enucleated human eye. Invest Ophthalmol Vis Sci. 1975;14:286-292.

79. Moses RA. The effect of intraocular pressure on resistance to outflow. Surv Ophthalmol. 1977;22:88-100.

80. Hashimoto JM, Epstein DL. Influence of intraocular pressure on aqueous outflow facility in enucleated eyes of different mammals. Invest Ophthalmol Vis Sci. 1980;19:1483-1489.

81. Johnstone MA, Grant WG. Pressure-dependent changes in structures of the aqueous outflow system of human and monkey eyes. Am J Ophthalmol. 1973;75:365-383.

82. Selbach JM, Posielek K, Steuhl KP, et al. Episcleral venous pressure in untreated primary open-angle and normal-tension glaucoma. Ophthalmologica. 2005;219:357-361.

83. Friberg TR, Sanborn G, Weinreb RN. Intraocular and episcleral venous pressure increase during inverted posture. Am J Ophthalmol. 1987;103:523-526.

84. Moster M, Ichhpujani P. Episcleral venous pressure and glaucoma. Journal of Current Glaucoma Practice. 2009;3:5-8.

85. Linnér E. The outflow pressure in normal and glaucomatous eyes. Acta Ophthalmol (Copenh). 1955;32:101-116.

86. Leith AB. Episcleral venous pressure in tonography. Brit J Ophthal. 1963;47:271-278.

87. Lohlein H, Weigelin E. Ueber den abfluss des kammerwassers am normalen und glaukom kranken Auge. Deutsch Ophthal Gesellsch. 1949;55:170-174.

88. Goldmann H. Der druck im Schlemmschen Kanal bei normalen und beiGlaucoma simplex. Experientia. 1950;3:110-111.

89. Rickenbach K, Werner H. Apparent drainage pressure, tension and pressure in the aqueous veins. Ophthalmologica. 1950;120:22-27.

90. Weigelin E, Lohlein H. Measurements of the blood pressure of the episcleral vessels of the eye in healthy persons. Albrecht Von Graefes Arch Ophthalmol. 1952;153:202-213.

91. Podos SM, Minas TF, Macri FJ. A new instrument to measure episcleral venous pressure – comparison of normal eyes and eyes with primary open-angle glaucoma. Arch Ophthalmol. 1968;80:209-213.

92. Talusan ED, Schwartz B. Episcleral venous pressure. Differences between normal, ocular hypertensive, and primary open angle glaucomas. Arch Ophthalmol. 1981;99:824-828.

93. Ellingsen BA, Grant WM. Trabeculotomy and sinusotomy in enucleated human eyes. Invest Ophthalmol Vis Sci. 1972;11:21-28.

94. Swaminathan SS, Oh DJ, Kang MH, et al. Aqueous outflow: Segmental and distal flow. J Cataract Refract Surg. 2014;40:1263-1272.

95. Zhou J, Smedley GT. Trabecular bypass: effect of schlemm canal and collector channel dilation. J Glaucoma. 2006;15:446-455.

96. Saheb H, Ahmed II. Micro-invasive glaucoma surgery: current perspectives and future directions. Curr Opin Ophthalmol. 2012;23:96-104.

97. Soohoo JR, Seibold LK, Radcliffe NM, et al. Minimally invasive glaucoma surgery: current implants and future innovations. Can J Ophthalmol. 2014;49:528-533.

98. Hays CL, Gulati V, Fan S, et al. Improvement in outflow facility by two novel microinvasive glaucoma surgery. Invest Ophthalmol Vis Sci. 2014;55:1893-1900.

99. Gabelt BT, Kaufman PL. Changes in aqueous humor dynamics with age and glaucoma. Prog Retin Eye Res. 2005;24:612-637.